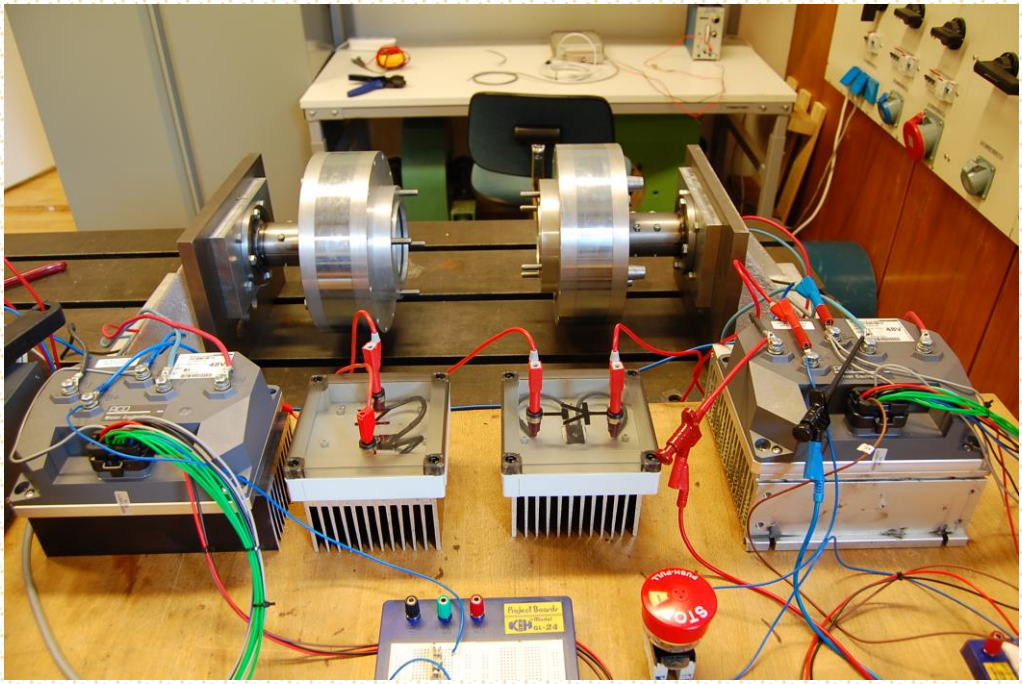

Leandro Camacho Silva

Modeling and Design of the Electric Drivetrain for the Research Concept Vehicle 2013

Departamento de Engenharia Eletrotécnica e de Computadores
Dissertação de Mestrado
Orientador: Aníbal de Almeida

27/09/2013

· U C ·

Universidade de Coimbra

KTH Electrical Engineering

Modeling and Design of the Electric Drivetrain for the 2013 Research Concept Vehicle

LEANDRO CAMACHO SILVA

Royal Institute of Tecknology
Department of Electrical Energy Conversion
Master Thesis in Electrical Machines and Drives
Supervisor/Examiner at KTH University: Oskar Wallmark
Supervisor at Coimbra University: Aníbal de Almeida

Stockholm September 2013
XR-EE-E2C 2013:008

Modeling and Design of the Electric Drivetrain for the 2013 Research Concept Vehicle
LEANDRO CAMACHO SILVA

School of Electrical Engineering
Department of Electrical Energy Conversion
Kungliga Tekniska Högskolan
SE–100 44 Stockholm
Sweden

To my family

Abstract

The research for electric vehicles has been growing during last years and the development of electric drive trains can be considered a main challenge. This thesis presents the electric drive train of the research concept vehicle (RCV) 2013, with particular focus on electric machines, motor controllers, and the communication system.

In the first part of this thesis, the electric drive train configuration and components are described. In-wheel motors are proposed which is a permanent magnet synchronous machine (PMSM). This technology allows the use of autonomous corner modules (ACM) increasing the quality and safety of the system. Each of the four in-wheel motors has a controller enabling the use of torque or speed control mode. Furthermore, an unit from the dSPACE company provides the total control of the system by CAN bus. Additionally, the dSPACE ControlDesk interface used to control the drive system is presented.

In the second part, the heat sink of the AC Drive is investigated by measurements and analytical calculations. Furthermore, the motor temperature at different loads is also presented and discussed.

Finally, the efficiency of an in-wheel motor (PRA 230) is studied. Also the efficiency of the motor controller is estimated and discussed. Furthermore, the projet described in this thesis was carried out in KTH university.

Key words: Control Area Network, Electric Drive Train, In-Wheel Motor, Permanent Magnet Synchronous Machine;

Resumo

Durante os últimos dez anos foi observado um grande aumento na investigação relativamente à área de veículos elétricos, levando a grandes desafios o desenvolvimento de novas tecnologias adequadas aos sistemas de tração.

Este trabalho pretende mostrar ao leitor o sistema de tração utilizado no veículo elétrico a ser desenvolvido na universidade ”Royal Institure of Technology”, conhecido como ”Research Concept Vehicle 2013”.

Na primeira parte desta dissertação é descrito o tipo de configuração do sistema de tração e os seus componentes. O sistema de tração é baseado em motores de ímanes permanentes integrados nas rodas (”in-wheel motors”). A presente configuração permite o uso dos módulos ACM (”Autonomous Corner Modules”) aumentando a segurança e a qualidade do sistema. Em cada um dos quatro motores integrados nas rodas é utilizado um controlador baseado no controlo de binário. Além disso, o controlo total do sistema de tração é feito através de um dispositivo (Microautobox 1401) da empresa dSPACE.

Seguidamente, é apresentado o modelo matemático utilizado para o dimensionamento de um dissipador de calor. Este, por sua vez, permite o arrefecimento do controlador do motor. São também apontadas medições da temperatura do motor e do seu controlador a diferentes cargas e velocidades.

Por fim, é estimado e discutido a eficiência de um dos quatro motores e do seu respetivo controlador. No último capítulo desta dissertação são, ainda, descritas as conclusões a que chegámos. A universidade ”Royal Institute of Technology” em Estocolmo, foi o local onde se desenvolveu o respetivo projeto descrito nesta tese.

Key words: Control Area Network, Electric Drive Train, In-Wheel Motor, Permanent Magnet Synchronous Machine;

Acknowledgements

First of all, I would like to thank my supervisor and examiner Assoc. Prof. Oskar Wallmark for his continuous support, encouragement during the project, and the important knowledge that he shared with me. I would also thank all the RCV Team, specially Dr. Peter Georén for his availability to help me and his good advices.

I further would like to thank Peter Lönn for his help regarding my laptop and software, the E2C laboratory technician Jesper Freiberg, and the E2C laboratory responsible Dr. Alija Cosic.

I am very grateful to Eng. Jörgen Rickan and Eng. Thord Nilson from Kollmorgen company. Their support and expertise was really important to accomplish my objectives.

I want to express my appreciation to all my friend in Sweden, Catarina, Sílvia, Pedro, Elisabeth, Mickael, Chris, Ann, Mathias... for sharing with me some part of their life with many unforgettable moments. Also thanks to my friends in Portugal, Andre, Nuno Carvalho, Nuno Pinheiro, Sofia, Rui, Pedro Marques... for giving me support and strengths during my stay in Stockholm.

Last, but certainly not least, I would like to express my deepest gratitude to my mother, sister, and brother for their continuous support and love during all my life. Without them I would not be who I am today and for sure this experience would not have been possible. Truly love you very much!

Leandro Camacho Silva
Stockholm, Sweden
August 2013

Contents

Chapter 1

Introduction

1.1 Motivation and objectives

Nowadays, electric vehicles (EVs) are becoming extremely important for transportation. As a matter of fact, fossil fuels are limited, which lead to seek new solutions to replace the traditional internal combustion engine vehicle (ICEV). Furthermore, the price of fuel is increasing constantly since last decade, due to the limited quantity of fossil fuels around the world. Thereby, the ambition of researchers is larger with the objective to reduce the fuel consumption and their emissions. Although, EVs is a promising technology that suits better in order to fulfill such aims. The strategy consists in the use of batteries and electric motors instead of fuel tanks and combustion engines.

The main components of EVs have been an important field of research. Engineers have been working hard by investigating different technologies regarding EVs in order to achieve safety, high performance, and comfort. In this sort of vehicles separated electric machines can be used instead of one large machine. They are usually placed one in each axle, or one in each wheel. The Autonomous Corner Modules (ACM) is based in a wheel hub by combining the drivetrain, suspension, brakes, steering, and an in wheel motor. This advanced technology helps to get rid of some mechanical parts of the traditional vehicle, for instance, axle, steering rod, etc. Although, the weight of the vehicle is significant reduced, and the space available is increased.

A common and famous architecture used to control all the drivetrain system in automation is the Controller Area Network (CAN) bus. CAN communication is relatively cheap, safe and reliable. Meanwhile, it consists of connecting all the electronic control units like sensors, actuators, motor controllers, etc... to the CAN bus in order to be possible to monitor and control all the devices.

The aim of this thesis is to design and investigate an electric drivetrain for the 2013 RCV being developed at Royal Institute of Technology (KTH). Focus will be given to the efficiency of its components, which were chosen according to the cost and technology. Indeed, major attentions are given to the in-wheel motors, its controllers, and the

communication system. Such components are investigated and presented in detail. Furthermore, analyses, simulations, and experimental results of the electric drivetrain system are compared and discussed.

This chapter also presents briefly the thesis outline, the Research Concept Vehicle, Permanent Magnet Synchronous Machines, Field-Oriented Control of a Surface-mounted PMSM, and CAN Communication in Automation.

1.2 Outline of the Thesis

This thesis has the following structure:

- Chapter 2 presents the electric drive train used in the RCV. The characteristics of the components are described in detail. The location of such components in the RCV platform is shown and discussed. How to initialize the CAN bus and how to tune the PI controllers of the motor controller is explained and presented in this chapter. Also, the dSPACE ControlDesk interface is shown and its main duty is explained.

- Chapter 3 presents some basics of thermal regarding semiconductors. After, the heat sink thermal resistance for the motor controller (ACD) is obtained, and experimental results are shown and discussed.

- Chapter 4 presents one possible method to estimate the efficiency of an in-wheel motor and ACD. Finally, the results obtained for the efficiency of the motor and ACD are presented.

- Chapter 5 summarizes the conclusions of the work and provides some proposals for further research.

1.3 Methodology and Material

In the first part of the project the necessary material for the electric drive train were chosen carefully. This was done based on the requirements of the RCV and the information collected. The motors and AC Drives (motor controllers) were the first ones to be chosen and ordered due to its importance on the system. After that, analytical calculations were carried out to observe the requirements of the material which are able to protect the system. During this stage, also material like connectors, contacts, bolts, cables, and others were obtained. The battery pack was being designed and modeled in parallel by a team member, due to the overload of work.

Next, the master controller of the system (dSPACE unit) was discussed and chosen. Truly, time was consumed by focusing in its software and hardware, which was of great

importance to control all the ECUs of the system. This task entailed the communication CAN open in automation which was studied in detail and implemented.

Later, the efficiency map of the in-wheel motors and ACDs were obtained by measuring a significant amount of samples of the power in different locations of the system. Thermal measurements were also observed and discussed.

As a matter fact, the behaviour of the ACDs were investigated and simulated, mainly its inverter (Pulse Width Modulation) and the torque control theories (Field-Oriented Control) behind. Finally, the control of all drive train was tested with a dSPACE unit by a model created in Matlab/Simulink.

1.4 Research Concept Vehicle

The Research Concept Vehicle is a novel project which aims to be energy efficient as possible. The research is being developed in the Laboratory of Electrical Energy Conversion by accomplishing the construction of the vehicle at the transports lab in KTH University. Additionally, there are involved different sort of researchers, specifically master students, PhD students, and senior researchers. The members of the RCV team have different tasks depending on their qualifications. There are the ones responsible for the construction of the following parts: the lightweight structure, the suspension system, the battery system, fluid dynamics and the main human interface (mechatronics). The electric drive train is the head of study of this thesis.

The architecture of the 2013 RCV needs to be innovative in order to achieve high-performance. Following, the technology of the concept vehicle is structured as follows [18]:

- Integration: Mechatronics built-in systems;
- Reduced weight: Light-weight, carbon fiber based chassis construction;
- Vehicle dynamics: Autonomous corner modules;
- Energy optimization: Autopilot/drive-management/platooning;
- Low electrical losses: High efficient, integrated motor and power electronics design;
- Safety: Crash avoidance system; Chassis design with crash-zone;

The first version of the RCV is dated to be accomplished in October of 2013. Meanwhile, the research is far away to be completed. The platform of the RCV is, in some way, flexible which allows new future improvements, or even more the installation of new electronic control units.

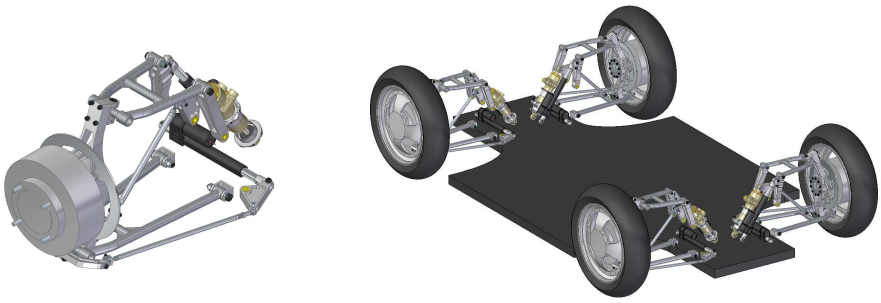

a) b)

Figure 1.1: a) Autonomous Corner Modules; b) Carbon Fiber Platform of the RCV 2013;

1.5 Autonomous Corner Modules

Autonomous corner modules is an advanced technology invented by Sigvard Zetterström at Volvo Car Corporation in 1998 [26]. In each ACM the forces and kinematics are controlled separately by actuators, electronic control units, and auxiliary software. The mechanical parts of the ACM are attached to the vehicle body, and its control is done by wire. The use of CAN communication is an easy way to control it from the master controller.

The safety of the system is optimized by controlling individually the torque of each wheel, load distribution and wheel angles [24]. Their efficiency is significantly higher than a normal wheel, but the complexity involved bring extra costs and attentions to the researchers involved. Furthermore, there is no need of mechanical steering and transmissions, which is an advantage of the technology evolved.

The design of the ACMs and the carbon fiber platform used by the RCV are shown in Figure 1.1.

1.6 Permanent Magnet Synchronous Machine

Permanent magnet synchronous motors (PMSM) are suitable for in-wheel drive applications due to their robustness and compactness. There are mainly three sorts of PMS motors. PMSM with surface magnets; the magnets are mounted on the surface of the rotor and it behaves as a smooth-air-gap machine because L_d=L_q (direct and quadrature synchronous inductances). In this sort of electrical machine the only torque produced comes from the magnets. PMSM with inset magnets has the magnets inset on the surface of the rotor and both synchronous inductances are different ($L_d \neq L_q$), which means that the total torque is the result of reluctance torque and magnet torque. The third one has the magnets buried in the rotor and it can have different geometries: radially or axially placed, or inclined. This machine is a salient-pole and $L_d \neq L_q$. Figure 1.2 shows two possible designs of inset and surface mounted magnets.

Three sort of common magnets used in PMSM are: ferrite, cobalt-samarium, and

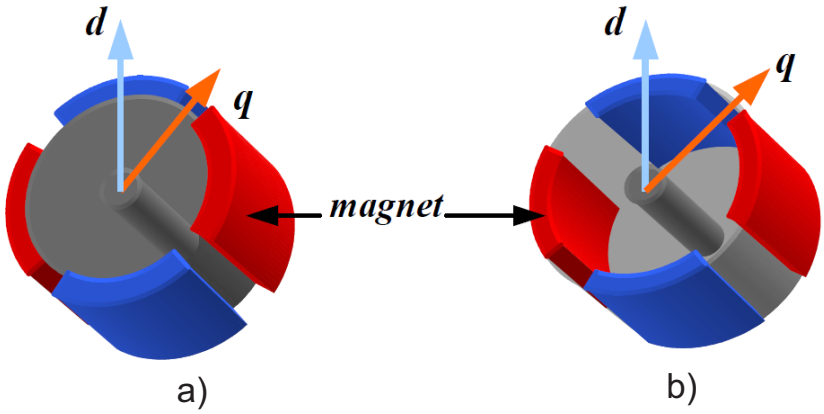

Figure 1.2: a) Surface mounted magnets (L_d=L_q); b) Inset mounted magnets ($L_d \neq L_q$) [5]

neodymium-iron-boron magnets. Neodymium-iron-boron magnet is the most used in PMSM for traction system, due to the high density value of energy. High power factor and torque density, low loss, and fast speed and torque response are its mains characteristics. Meanwhile, there are some drawbacks concerning permanent magnets, for instance high cost, temperature limitation during operation, and possibility of demagnetization.

1.6.1 Basics of Surface-mounted PMSM

Electromagnetic Torque

In a surface-mounted PMSM the instantaneous electromagnetic torque is given by equation 1.1 [19]:

$$T_e = \frac{3}{2} p \psi_m i_s \sin \beta \tag{1.1}$$

where p is the number of pair poles, ψ_m is the magnet flux, i_s is the stator current, and β is the torque angle electrical angle between the stator magnetomotive force (d axis) and the rotor angle ($\beta = \alpha_s - \theta_r$). The rotor angle is the angle between the magnet flux in the d axis of the rotor, and the d axis of the stator reference frame. The respective current vector is shown in Figure 1.3.

There are different possibilities to express equation 1.1. However, the maximum torque of the machine is given when the torque angle is equal to $90°\mathrm{C}$. Equation 1.1 also shows that the electromagnetic torque is proportional to the stator current and magnet flux. The magnet flux is a constant and it depends on the characteristics of the magnet mounted. Meanwhile, the stator current can be easily controlled by using a current-controlled PWM inverter in order to obtain fast torque response [20].

The stator current vector in the rotor reference frame is obtained by equation 1.2:

$$i_s = i_d + j i_q = |i_s| \sin(\alpha_s - \theta_r) \tag{1.2}$$

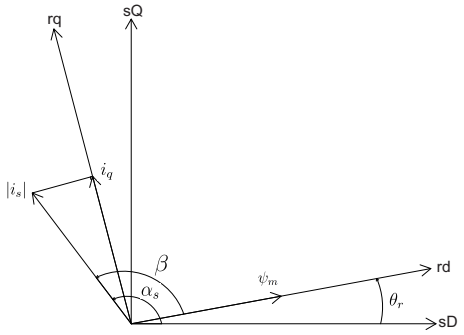

Figure 1.3: Current vector diagram of a surface-mounted PMSM (rotor-oriented control)

The component i_d is assumed to be zero when operating in the region of maximum torque. Field weakening region is for speeds above the rated speed and it is necessary a negative value of i_d. Meanwhile, the stator current component is shown in equation 1.3.

$$i_q = |i_s| \sin(\alpha_s - \theta_r) \tag{1.3}$$

Therefore, the electromagnetic torque can be controlled if the stator current components and the rotor angle are known. It can be obtained by measuring the current and using a position sensor.

Back Electromotive Force

The back electromotive force (BEMF) is the voltage induced in the stator windings of the motor/generator due to the presence of a magnet field. If it is operating as a motor, the BEMF opposes the voltage applied in the stator windings. The BEMF in a 3-phase stator windings without an external applied voltage is given by the following equations:

$$V_{an} = \omega_e \psi_m \sin(\omega t) \tag{1.4}$$

$$V_{bn} = \omega_e \psi_m \sin(\omega t + 120) \tag{1.5}$$

$$V_{cn} = \omega_e \psi_m \sin(\omega t + 240) \tag{1.6}$$

where ω_e is the electric speed in rad/s ($\omega_e = 2\pi \frac{n}{120} p$).

There is the possibility to calculate the magnet flux by measuring phase to phase voltage. If it is the case, the magnet flux is obtained as follows:

$$\psi_m = \frac{V_{pp}}{\sqrt{3}\omega_e} \tag{1.7}$$

were V_{pp} is the fundamental value of the phase to phase voltage.

Load and Motor Inertia

The total electromagnetic torque by including the load and motor inertia is given by equation 1.9:

$$\frac{d\omega}{dt} = \frac{T_e - T_L}{J_M + J_L} \tag{1.8}$$

$$T_e = T_L + (J_M + J_L)\frac{d\omega}{dt} \tag{1.9}$$

where J_M is the motor inertia, J_L is the load inertia, and ω is the angular speed of the motor.

1.7 Field-Oriented Control of a Surface-mounted PMSM

In this section it will be shown the principle of field-oriented control. Also, simulations results are presented to observe the behaviour of the machine.

1.7.1 Introduction

In the last years, several torque control topologies have been investigated. This topologies tend to improve the dynamic performance of an electrical machine. The most common ones are mainly field-oriented (FOC) and direct-torque control (DTC). The DTC is based on hysteresis controllers to control the torque and flux of the machine. Such control does not need an inverter (PWM modulator), since the control is done by an optimal switching logic. In this thesis it is studied FOC which was introduced in Germany by Blaschke, Hasse, and Leonhard [20]. In FOC, the spatial angular position of the rotor flux is required by the drive. The control is based on a comparison of the known stator field vector and the feedback rotor position and speed. In this case, the respective surface-mounted PMSM are mainly modeled in the $d-q$ reference frame facilitating the control strategy implementation [10]. In this control strategy, the electromagnetic torque reference T_{eref} is proportional to i_s, due to the fact that $T_e = \frac{3}{2}p\psi_m i_s \sin\beta$. Below the rated speed, $i_d = 0$ and $i_s = i_q$, because the maximum torque is available (torque angle equal to $90°$). Furthermore, the stator current is controlled by one PWM inverter. If the speed is above the rated, the machine is in field weakening range and the limit of the inverter voltage was achieved. Moreover, a negative value of i_{dref} is provided which increases the torque angle more than $90°$. Since the stator current modulus is give by equation 1.10, its modulus should be lower that the maximum allowed value (i_{smax}).

$$|i_s| = \sqrt{i_d^2 + i_q^2} \leq i_{smax} \tag{1.10}$$

So the component of the stator current i_q, may need to be decreased, which limits the torque available (T_{eref}).

1.7.2 Mathematical Model of a Surface-Mounted PMSM

There are different possibilities to analyze electric control of a PMSM. A common and reliable one is the d-q axis mathematical model. Such model is based in voltage equations, electromagnetic torque equation, mechanical dynamics equation, and the stator flux linkage equations [22]. From the three-phase sinusoidal system (f_{as}, f_{bs}, and f_{cs}), the currents, voltages, and fluxes are transformed into 2-phase system (f_d and f_q) (rotor reference frame). This is done by using the famous Park transformation which facilitates the implementation of a three-phase system model. Therefore, the transients and the steady state of a PMSM are studied by using space-phasor theory [20]. A simple vector diagram of a two-pole PMSM three phase system can be seen in Figure1.4. The vectors sD and sQ are in the stationary reference frame and is the same as the well known α and β coordinates.

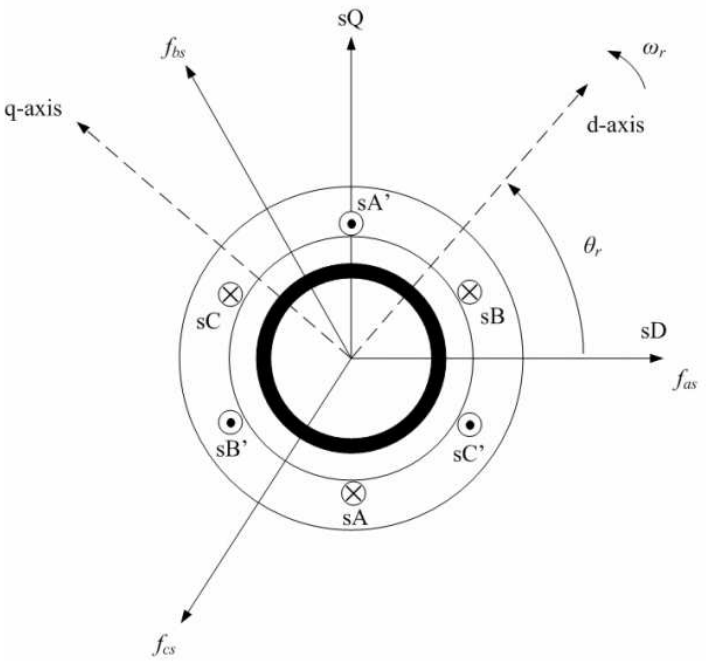

Figure 1.4: Simplified cross-section of a two-pole PMSM [4].

1.7.3 Park Transformation

The Park transformation was introduced in 1920 by R. H. Park in order to facilitate the analyze of three-phase circuits. In electrical machines, the symmetrical three-phase stator windings are transformed in two DC components (I_d and I_q) as explained before. Such transformation angle θ, is the angle between the vector f_{as} and the $d-axis$ which can be seen in Figure 1.4 as θ_r. In PMSM, the $d-axis$ is common fixed on the magnetic north pole of the rotor magnet [21]. The $d-q$ components expressed as a vector are presented

as follows:

$$\begin{bmatrix} f_d \\ f_q \\ f_0 \end{bmatrix} = \mathbf{T}_{park,dq} \begin{bmatrix} f_{as} \\ f_{bs} \\ f_{cs} \end{bmatrix} \tag{1.11}$$

where the Park transformation is $\mathbf{T}_{park,dq}$ and given by matrix 1.12.

$$\mathbf{T}_{park,dq} = \frac{2}{3} \begin{bmatrix} cos\theta & cos(\theta - \frac{2\pi}{3}) & cos(\theta + \frac{2\pi}{3}) \\ -sin\theta & -sin(\theta - \frac{2\pi}{3}) & -sin(\theta + \frac{2\pi}{3}) \\ \frac{1}{2} & \frac{1}{2} & \frac{1}{2} \end{bmatrix} \tag{1.12}$$

The f_0 component is assumed to be zero for electrical machines with symmetrical three-phase stator windings [21]. In this case the amplitude of the variables f_{as}, f_{bs} and f_{cs} is given by $\sqrt{f_d^2 + f_q^2}$.

1.7.4 Voltage and Current dynamics

For PMSM two-phase system (direct and quadrature axis) the $d-q$ voltages are given by the sum of the resistive voltage drops and the derivative of the flux linkages in the respective windings. In the rotor reference frame, such voltages are given by the following equations 1.13 and 1.14 [21].

$$V_d = R_s i_q + L_d \frac{di_d}{dt} - \omega_r L_q i_q \tag{1.13}$$

$$V_q = R_s i_q + L_q \frac{di_q}{dt} + \omega_r L_q i_q + \omega_r \psi_m \tag{1.14}$$

In this case, the voltages are computed by neglecting all the harmonics of the flux linkage and inductance [21]. Furthermore, the back EMF voltage is assumed to be sinusoidal. For a non-salient PMSM studied in this thesis, the q-axis and d-axis stator inductance are both equal. The flux equations in the $d-q$ rotor reference frame is given as follows:

$$\psi_d = L_d i_d \tag{1.15}$$

$$\psi_q = L_q i_q \tag{1.16}$$

$$\psi_m = L_m i_m = \frac{V_{pp}}{\sqrt{3}\omega_r} \tag{1.17}$$

The cross-coupling ($-\omega_s L_q i_q$ and $+\omega_s L_d i_d$) between the $d-q$ axis shown in equations (1.13) and (1.14) has a negative effect on the transient control. For instance, the current rise time will be slow down [19]. This is due to the fact that when the current i_q is increased, it affects the voltage in the q and d axis.

1.7.5 Electromagnetic Torque and Mechanical Dynamics

The electromagnetic torque of a salient PMSM in the rotor reference frame is given by equation 1.19 [19]:

$$T_e = \frac{3}{2}p[\psi_m i_q + (L_d - L_q)i_d i_q] \tag{1.18}$$

For a non-salient PMSM the electromagnetic torque equation simplifies to

$$T_e = \frac{3}{2}p\psi_m i_q \tag{1.19}$$

which was already known from section 1.6. The mechanical dynamics equation which describes the whole machine, as in section 1.6 is [21]

$$\frac{d\omega_r}{dt} = \frac{p}{J}(T_e - \frac{B_m}{p}\omega_r - T_L) \tag{1.20}$$

$$\frac{d\theta_r}{dt} = \omega_r \tag{1.21}$$

where B_m is the viscous friction coefficient.

Finally the surface-mounted PMSM mathematical model is given by the equations described before: 1.13,1.14,1.19, 1.20 and 1.21.

1.7.6 Voltage and Current Limits

In a surface-mounted PMSM the maximum torque obtained is limited by the maximum current allowed and the DC-Link voltage available. Such limitations are given by the following conditions:

$$\sqrt{i_d^2 + i_q^2} \leq i_{max} \tag{1.22}$$

$$\sqrt{v_d^2 + v_q^2} \leq \frac{u_{dc}}{\sqrt{3}} = u_{max} \tag{1.23}$$

Assuming the resistive voltage drops are zero and substituting v_d and v_q in equation 1.23, the following condition is achieved:

$$[(\frac{\psi_m}{L_s} + i_d)^2 + (i_q)^2] \leq \frac{u_{max}}{\omega_r^2 L_s} \tag{1.24}$$

where

$$v_d = -\omega_r L_s i_q \tag{1.25}$$

$$v_q = \omega_r(L_s i_d + \psi_m) \tag{1.26}$$

$$L_s = L_q = L_d \tag{1.27}$$

From equation 1.24 it can be concluded that the trajectory of the stator voltage is a set of circles. These circles are centered on $(\frac{-\psi_m}{L_s}, 0)$ and radius equal to $\frac{u_{max}}{\omega_r^2 L_s}$ in the $d-q$ coordinate system. Meanwhile, Figure 1.5 shows the drive's voltage and current-limit constraints in the $d-q$ coordinate system for a PMSM. If the motor follows the red line, the maximum torque is obtained at different speeds ($i_d = 0$ and $i_q \neq 0$). The green lines represents different torque values at constant speed. In field weakening region the current i_d should be controlled in order to reduce the voltage magnitude.

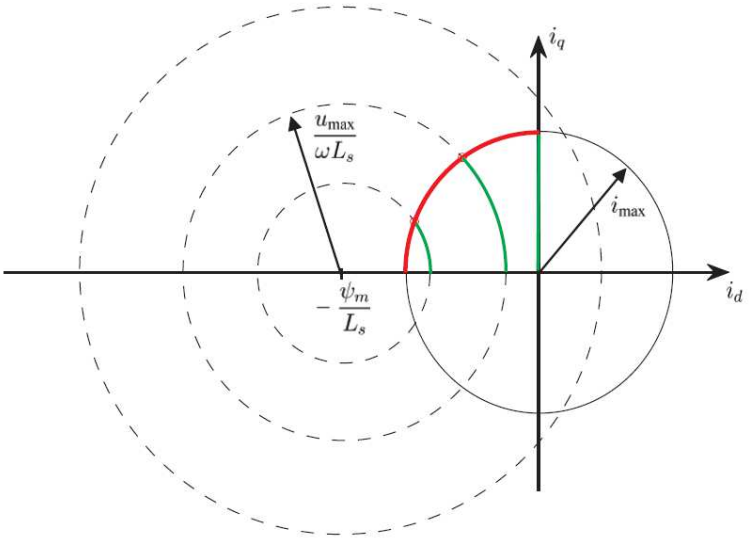

Figure 1.5: Circle diagram with field weakening technique [16].

1.7.7 Design of the Current Controllers

The design of current controllers have a significant impact on the performance of the drive system. A common and accurate strategy is to use Proportional and Integral controllers in a PWM inverter-fed PMSM. In this case, it is well known that the electric dynamics, such as their time constants, are much faster than the mechanical time constants. Furthermore, the mechanical speed of a motor is constant during the switching period of an inverter. The electromagnetic torque of a surface-mounted PMSM is proportional to the stator current (i_s), which means that the quality of the speed and torque is dependent of the current controllers. A well designed current-controller PWM converter has, mainly, the following characteristics [11]:

- Instantaneous control of the current waveform and high accuracy;

- Protection against peak currents;
- Overload rejection;
- Compensation of the dc-link and ac-side voltage changes;
- Extremity good system dynamics;
- Compensation of the semiconductor voltage drop and dead times of the converter;
- Compensation of effects due to load parameter changes (resistance and reactance);

For a surface-mounted PMSM, the current PI controller is based on the following equations [21]:

$$V_d^{ref} = k_{p,d}(i_d^{ref} - i_d) + k_{i,d}\int (i_d^{ref} - i_d)dt - \omega_r L_q i_q - R_{a,d} i_d \tag{1.28}$$

$$V_q^{ref} = k_{p,q}(i_q^{ref} - i_q) + k_{i,q}\int (i_q^{ref} - i_q)dt - \omega_r L_d i_d - R_{a,q} i_q; \tag{1.29}$$

The first two terms of the equation are the respective PI controller and the last term is to compensate the coupling terms of equations 1.13 and 1.14. The integral and proportional gains of both $d-q$ components are given by:

$$k_{p,d} = \alpha_c L_d, \quad k_{p,q} = \alpha_c L_q \tag{1.30}$$

$$k_{i,d} = \alpha_c (R_s + Ra, d), \quad k_{i,q} = \alpha_c (R_s + Ra, q) \tag{1.31}$$

were α_c is the respective closed loop bandwidth, and is obtained by equation 1.32.

$$\alpha_c = \frac{ln(9)}{t_r} \tag{1.32}$$

The variable t_r is the rise time of the current step response. Figure 1.6 shows the block diagram of the closed-loop current dynamics.

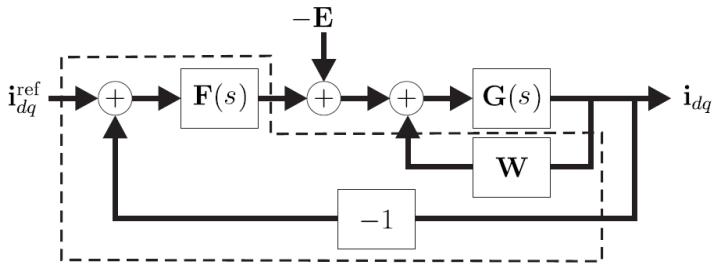

Figure 1.6: Block diagram of the current dynamics [21]

From the block diagram, the current PI controller is represented as $\mathbf{F}(p)$, the decoupling and active damping as $\mathbf{W}(p)$, the open-loop transfer function as $\mathbf{G}(p)$, and the back EMF transfer function $\mathbf{F}(p)$.

$$\mathbf{F}(s) = \begin{bmatrix} k_{p,d} + k_{i,d}/s & 0 \\ 0 & k_{p,q} + k_{i,q}/s \end{bmatrix} \tag{1.33}$$

$$\mathbf{W}(s) = \begin{bmatrix} -R_{a,d} & -\omega_r L_q \\ \omega_r L_d & -R_{a,q} \end{bmatrix} \tag{1.34}$$

$$\mathbf{G}(s) = \begin{bmatrix} \frac{\alpha_c}{s+\alpha_c} & 0 \\ 0 & s + \alpha_c \end{bmatrix}^{-1} \tag{1.35}$$

$$\mathbf{F}(s) = \begin{bmatrix} 0 & \omega_r \psi_m \end{bmatrix}^T \tag{1.36}$$

The closed-loop transfer function should be tuned by setting the correct gains ($K_p = \alpha_c L$ and $K_i = \alpha_c R$). The first step is to choose a desired controller bandwidth (α_c), and the gains will be obtained by equations 1.30 and 1.31. According to the rise time, the bandwidth of the system should not be too high due to the system sampling time. The main rule is to choose a bandwidth 5-10 times slower than the system sampling time (T_s) [8].

1.7.8 Simulations Results

The contents presented in this sections were carried out based in a model created in Matlab/Simulink.

The in-wheel motor used in the RCV 2013, was modeled in Matlab/Simulink software together with the current-controller PWM converter. Figure 1.7 shows the Simulink model used to simulate the drive system.

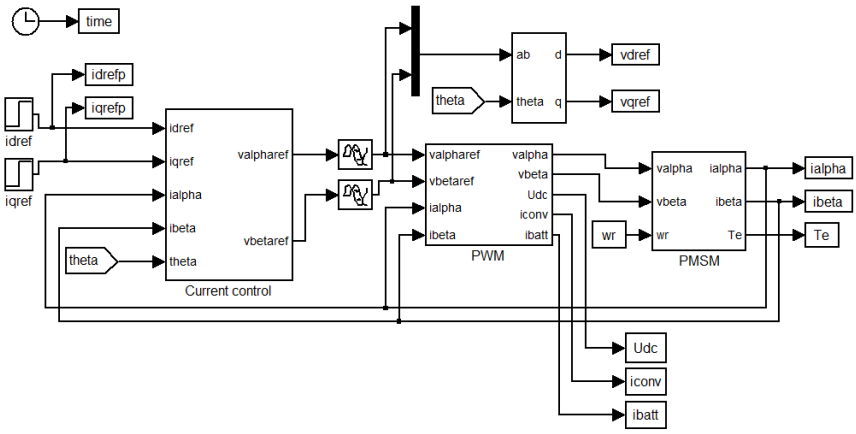

Figure 1.7: Drive system model in Simulink.

In this simulations it was chosen a rise time equal to $5ms$. Other important parameters were based in an in-wheel motor (PRA 230) which is presented in chapter 2. The step response of the current i_q, and the stator three phase current is shown in figure 1.8 with a load of 33Nm and for speed equal to 150 rpm. The current i_d is set to be zero due to the fact that the motor is operating below rated speed. The DC link voltage, the limit voltage, and the amplitude of the stator voltage is shown in Figure 1.9.

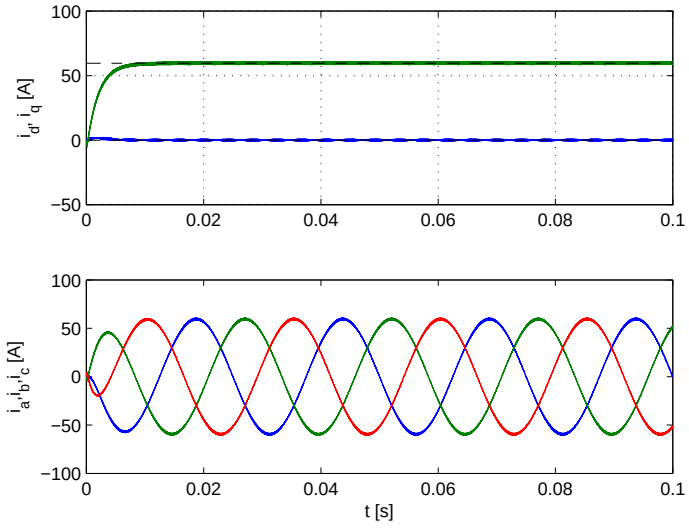

Figure 1.8: Current step response and stator currents at rated torque and 150 rpm.

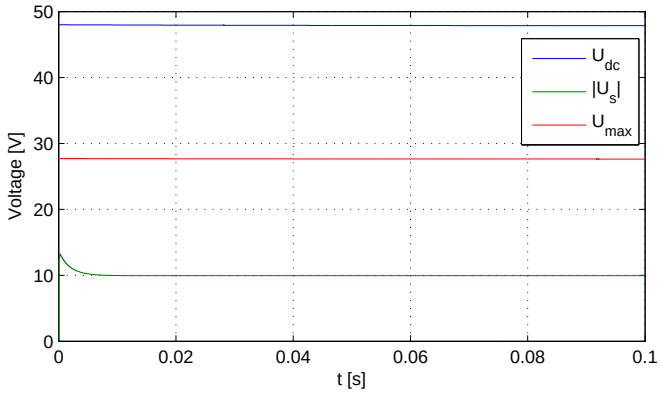

Figure 1.9: Limit voltage, DC link voltage, and stator voltage at rated torque and 150 rpm.

Figures 1.10 and 1.11 shows the simulation results at rated torque and speed. In this case, the inverter is working on over modulation range due to the low value of the DC link voltage. Also, it is possible to observe some distortion on the current wave. To avoid PWM over modulation, field weakening should be implemented, or the DC link voltage should be increased until the maximum range allowed.

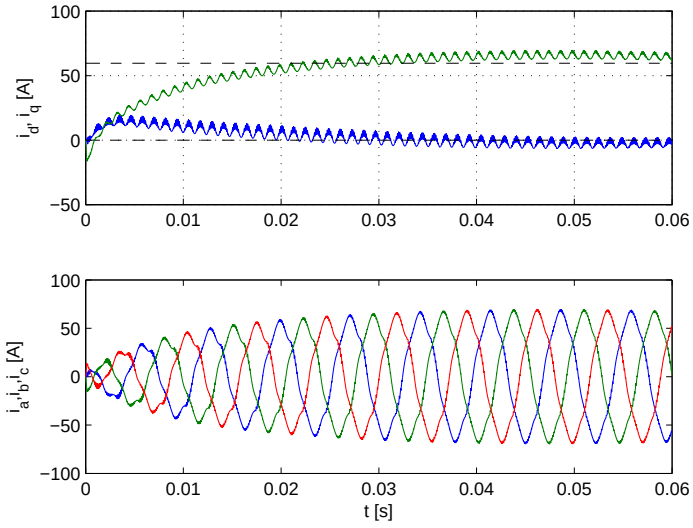

Figure 1.10: Current step response and stator currents at rated torque and speed.

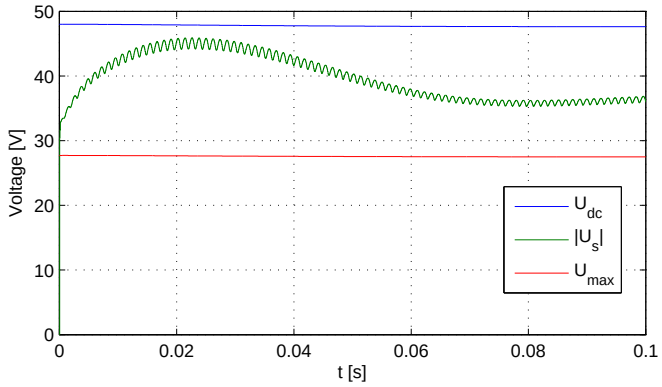

Figure 1.11: Limit voltage, DC link voltage, and stator voltage at rated torque and speed.

1.8 CAN Communication in Automation

There are several types of communication network used in automation. For instance: CAN protocol, LIN (Local Interconnect Network) protocol, the Flexray protocol, and MOST (Media Oriented Systems Transport) protocol. In this thesis it is studied CAN communication network due to the use of CANopen on the electric drive train of the RCV. Indeed, the following principles of CAN communication were resumed from the documents [17], [15], [1], and [3].

CAN bus is a serial data communication protocol invented by BOSCH corporation. In serial data communication, all the electronic devices share the same communication medium (CAN bus), where the control, address, and data are transmitted on the same bus. Furthermore, such information is transmitted serially bitwise, and the identified node or nodes (electronic devices) receive the message. The costs, weight and space of a CAN bus system are reduced compared to the traditional parallel data communication. Also, CAN bus protocol should be able to avoid data collision, loss or even blocking of information. Indeed, it is a potential communication network used in automation, health care, agriculture and others.

In automotive there are a large number of electronic control units (ECUs) which constitutes different subsystems. The biggest control unit in vehicles is the Engine Control Module (ECM), or Powertrain Control Module (PCM). Auxiliary subsystem which are common controlled by CAN bus is the battery and the recharging system for electric or hybrid vehicles, doors, mirrors adjustments, electric power steering (EPS), audio systems and others.

In CAN bus there are the possibility to use double stranded wire, coaxial cable or optical fiber for the communication medium [17]. Depending on the CAN controller the speed can be up to $1Mbps$. A simple diagram showing the CAN bus topology is shown in

Figure 1.12.

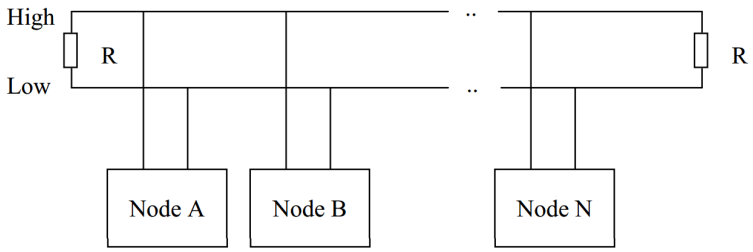

Figure 1.12: CAN bus diagram.

The CAN transmission medium is constituted by the high level transmission line (CANH) and the low level transmission line (CANL).

1.8.1 CAN Bus Communication Network Model

From Figure 1.12, each node is able to transmit and receive messages. Each message is transmitted serially, not simultaneously, and it has an identifier (ID) representing the priority of the message. The electronic control units, for instance sensors and actuators, are connected to the CAN bus through a host processor and a CAN controller. The host processor examines carefully which messages will be received and which ones will be transmitted. The CAN controller stores serially the bits being received until a message is constituted. Also, the CAN controller transmits serially to the CAN bus, the messages chosen by the host processor. When a conflict is detected, the message with more dominate bits (zeros) will have priority and is the first to be transmitted to all nodes.

There are two types of CAN frame: standard frames (11 bits message identifier) and extended frame (29 bits message identifiers). It is possible to have both CAN frames in the same bus. The CAN frame implemented by the ACD 4805 is standard frames and is shown in Figure 1.13.

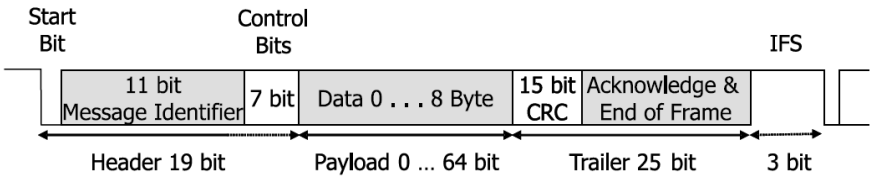

Figure 1.13: CAN Frame Structure [15].

In 1993, CAN became an International Organization for Standardization standard (ISO-11898). The ISO-11898 standard, CAN 2.0, is the most used physical layer for

CAN networks. The CAN protocol is based on the OSI-7 layer reference model which can be seen in Figure 1.14. SAEJ1939 is a high level communication network protocol used in automotive. It was developed by the Control and Communications Network Subcommittee, Society of Automotive Engineer-Trucks and Buses Electrical and Electronics Committee [17]. This protocol is constituted by four layer: physical layer, data link layer, network layer and application layer.

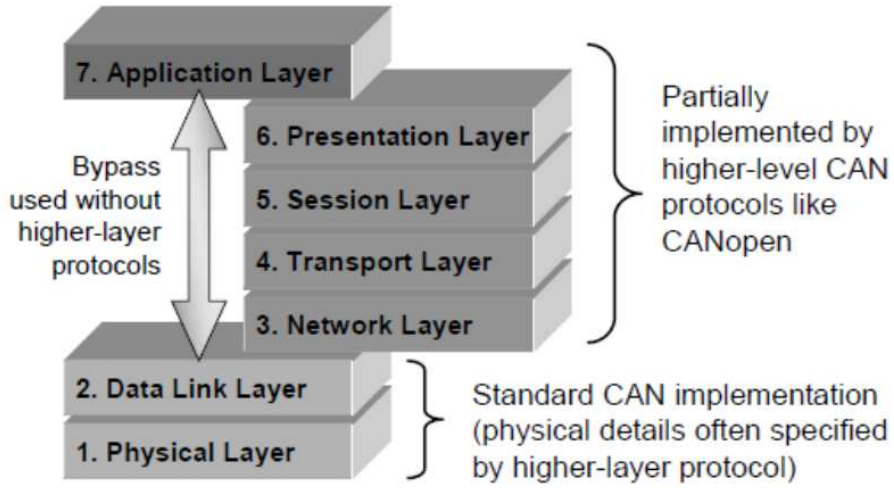

Figure 1.14: CAN protocol and OSI-7 layer reference model [15].

Physical Layer

The physical layer is constituted by electric devices, cables, pin layouts, level of voltage, signal timing, and others. Also, Bit-Encoding, Bit-Timing and synchronisation, and the communication medium is specified by the physical layer. A possible CAN structure diagram can be seen in Figure 1.12. In each end of the circuit is recommended to have a resistance equal to 120Ω to avoid reflection and loss of signal. The CAN bus length is based on the baud rate chosen. All the devices connected to the CAN bus should have the same baud rate to be able communication between each other.

Data link Layer

The data link layer is situated between the physical and the network layer. This layer can be divided in two sublayers: the Logical Link Control (LLC) and the Multiple Access Control (MAC) sublayer. The LLC sublayer is responsible to detect and if possible correct the errors that may occur in the physical layer. The MAC sublayer handles the access to the bus in other to avoid collision when different nodes try to transmit messages simultaneously. The data link layer also specifies the format length of the message, extended or standard frames (Fig. 1.13).

Application Layer

The application layer provides several services and protocols useful to all the devices on the system. It provides direct process when the end user wants to transfer files, send emails or implement other network related activities.

1.8.2 CANopen Protocol

CAN open is a communication protocol of high level used in automation, which the standard consists on several protocols and an application layer defined by a device profile. The communications protocols are able to support the network management, monitoring, and communication between each element of the bus. Also, includes a transport layer for coding and decoding of messages. The data link layer and the physical layer are implemented by the lower level protocol CAN. The overall diagram of the system is shown in Figure 1.15. The communication and device profiles are given by CiA 301 specification.

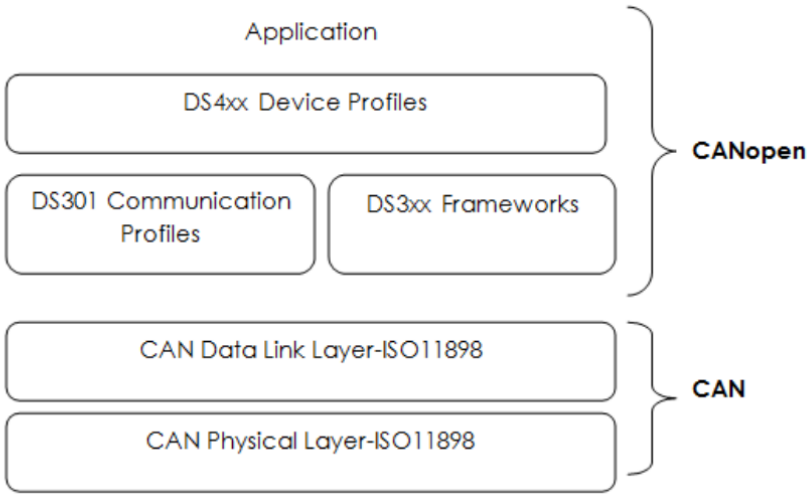

Figure 1.15: Diagram of the CAN and CANopen protocol [17].

Device Model

Each device that uses CANopen protocol should have a communication unit which implements protocols for messaging between nodes. A state machine controls the device, being able to start and reset it. Also the following states are available on the device: Initialization, Pre-operational, Operational and Stopped.

CANopen devices have implemented in its software an object-dictionary (OD) which allows the configuration and communication by the user. In other words, the OD contains all parameters describing the device and its network behaviour.

Object Dictionary (OD)

The OD is composed by a group od objects; each object is addressed using a 16-bit index. Also, individual structured data elements can be accessed by a 8-bit subindex. Figure 1.16 shows the CANopen OD layout. It is important to know that the relevant range of OD node's is between 1000 and $9FFF$. The device parameters are described in the document provided by the manufacturer facilitating its access via CAN bus. Each parameter of the object dictionary has the following profile: its name, its index and sub-index, its data type, mandatory or optional, read-only or write-only or write/read, etc.

CANopen Object Dictionary	
Index	**Object**
0000	*not used*
0001 - 001F	Static Data Types (standard data types, e.g. Boolean, Integer16)
0020 - 003F	Complex Data Types (predefined structures composed of standard data types, e.g. PDOCommPar, SDOParameter)
0040 - 005F	Manufacturer Specific Complex Data Types
0060 - 007F	Device Profile Specific Static Data Types
0080 - 009F	Device Profile Specific Complex Data Types
00A0 - 0FFF	*reserved*
1000 - 1FFF	Communication Profile Area (e.g. Device Type, Error Register, Number of PDOs supported)
2000 - 5FFF	Manufacturer Specific Profile Area
6000 - 9FFF	Standardised Device Profile Area (e.g. "DSP-401 Device Profile for I/0 Modules" [3]: Read State 8 Input Lines, etc.)
A000 - FFFF	*reserved*

Figure 1.16: CANopen Object Dictionary structure (index in hexadecimal) [3].

1.8.3 CANopen Communication Model

The CANopen communication model is defined by four types of messages, which are characterized by their CAN object identifier (COB-ID) and CAN-Identifier.

1 - Administrative message

The objective of these messages is to provide network and layer management, and identifier distribution of services. Services and protocols of administrative message are according to the service elements of CAL (CAN Application Layer): Network Management (NMT), Layer Management (LMT) and Distributor (DBT).

2 - Service Data Object (SDO)

The SDO protocol is used for writing and reading values from the object dictionary of a device. For that there is a need of a SDO client and a SDO server. The SDO client is the device which access the remote device, for instance dSPACE unit; the SDO server

is the device with the OD being accessed. The communication between both is always initialized by the SDO client.

In CANopen communication an upload from a parameter of the OD is known as a SDO upload, and a write is known as a SDO download. Also, there is a need to set the CAN object identifier of the SDO message transmitted from the server to client and the client to server. This can be done on the object dictionary of each remote device. Furthermore, it is possible to have 128 SDO servers, and it can be set up with addresses 0x1200h to 0x127Fh. Similar, 128 SDO clients are possible and respective addresses are between 0x1280 to 0x12FFh. There is also a pre-defined connection set which defines a SDO channel allowing the configuration of the device even during the operation. The COB-ID of this channel is 0x600h + node ID for receiving and 0x580h + node ID for transmitting. Figure 1.17 shows the SDO frame. If it is a SDO for reading a parameter of the OD, the data field should be zero and byte 1 equal to 40h. In case of a SDO for writing byte 1 should have the value of 2Bh when writing exactly 2 bytes. It is important to know that byte 1 depends of the data length (byte 5 to 8); detailed information can be found in [1]. The index and sub index can be found on the manual of the object dictionary. Moreover, each SDO message is only able to access only one parameter of the object dictionary.

Arbitration Field	Data Field							
COB-ID	Byte 1	Byte 2	Byte 3	Byte 4	Byte 5	Byte 6	Byte 7	Byte 8
600 or 580 + Node-ID*	Data Specification	Object Index (LSB)	Object Index (MSB)	Sub-Index	Data			

Figure 1.17: SDO frame [1].

3 - Process Data Object (PDO)

PDO protocol is used to transmit real time data between various nodes. There is the possibility to transmit or receive up to 8 bytes of data per each PDO message. Also, it is possible to access multiple parameters of the object dictionary by using only one PDO message.

There is two types of PDO messages: the receive PDO (RPDO) and the transmit PDO (RPDO). The TPDO is the message sent by the node (server) to the host (client), and the RPDO is the message sent by the host to the node (write or read). Similar to the SDOs, each of these messages have different COB-IDs, and it can be up to 512.

4 - Predefined messages or Special Function Objects

These special function has the object to monitor and provide axillar control of the network. For instance:

- Synchronization (SYNC);

- Time Stamp;
- Emergency;
- Node/Life Guarding.

Chapter 2

The Electric Drive Train of the RCV 2013

This chapter starts presenting different sort of drive trains for EVs. After, it is explained why the use of wheel hub motors for the RCV. After, several drive train components of the RCV are described, and setting out their importance and duty of the system. The gains of the PI controllers are tuned and presented in this chapter. Also, the dSPACE ControlDesk interface is shown and explained.

2.1 Drive train configurations

The development of new concept vehicles require drive trains appropriated, and as well sophisticated. There is a variety of multiple choices for battery electric vehicles (BEV). Indeed, depending on the drive train approach different vehicle dynamics are offered.

The electric drive train should be chosen based on the number of electrical machines, the energy storage system, the space and weight limitations, and other vehicle parameters and requirements. Figure 2.1 shows different topologies possible for the RCV.

In fact, the electric drive train of the RCV was based in the following criteria: total cost, safety, efficiency, space and weigh required, vehicle dynamics, and the master controller available. Accordingly, wheel hub electrical machines (Autonomous Corner Modules), without mechanical transmission, was the technology chosen.

2.2 RCV 2013 Architecture

2.2.1 Power Drive Train System

The electric drive train of the RCV can be separated in two subsystems. There is the power drive train and the control drive train. The power drive train diagram is shown

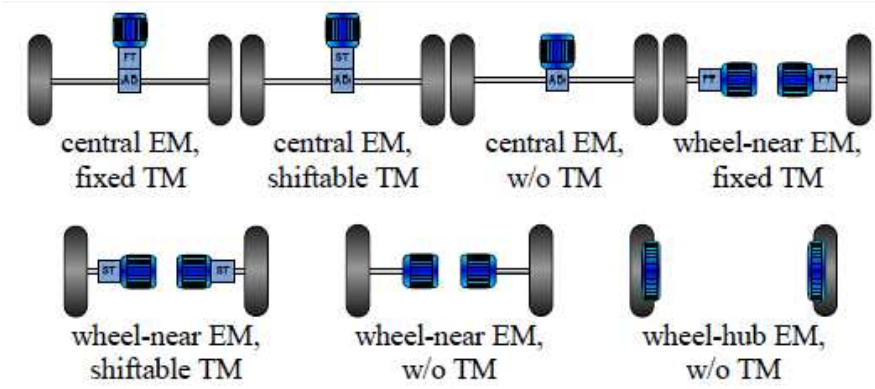

Figure 2.1: Drive trains configurations for EVs [7]

in Figure2.2. The system is constituted by four in-wheel motors, four AC Drives, one contactor, one emergency button, one large fuse, and one battery pack. The emergency button should be placed near the drive and after the contactor. The contactor is a Kilovac unit and it has a maximum current and voltage of 500A and 900V DC. The coil voltage has a range of 9 to 36 V. In order to protect the system, a fuse of 200A was installed, and also the logic of each ACD is protected with one fuse of 1A. The location of each component should be placed wisely in order to avoid electromagnetic interferences. Indeed, it is of great importance that the designer provides solutions to reduce the disturbances of the electrical contacts and between electrical components. The motor and battery cables were separated from the signal cables, but in some cases it was not possible to avoid their intersection. Therefore, when the cables cross each other, it should be placed at 90 degrees angle between both [19].

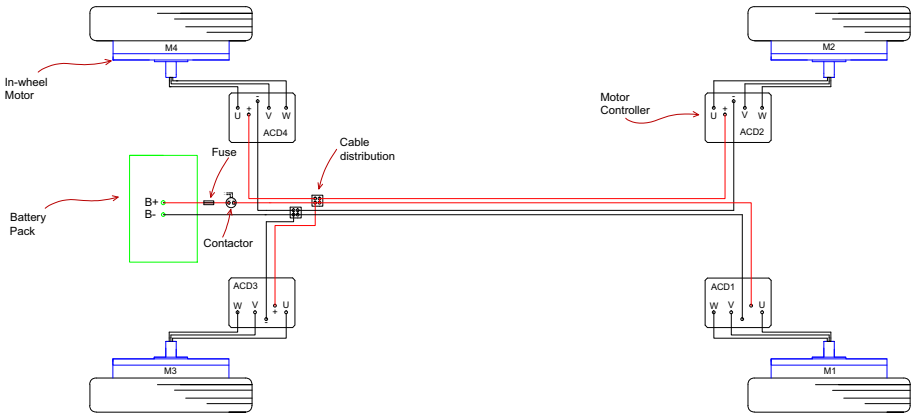

Figure 2.2: Power drive train system of the RCV 2013.

.

2.2.2 Control Cabling and Electronic units of the Drive Train System

The control cabling and electronic units of the drive train diagram can be seen in Figure 2.3. The separation of the control drive train and power drive train diagrams facilitates the reader to understand it.

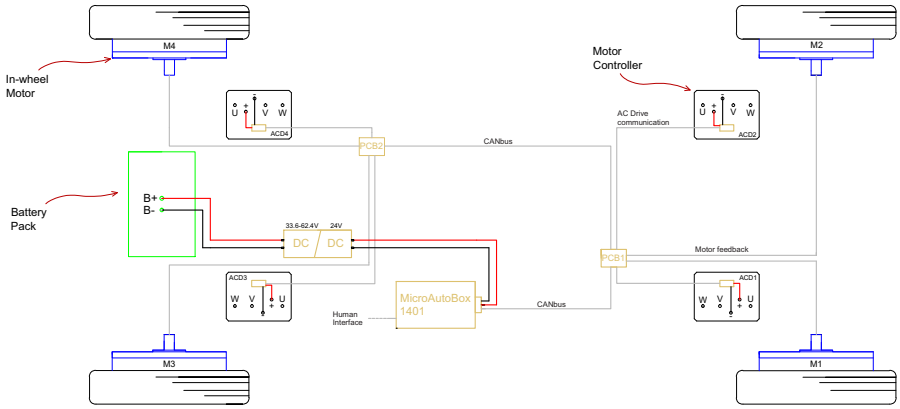

Figure 2.3: Control cabling and electronic units of the RCV 2013.

The communication between the master unit and the slave units is done by CANopen protocol, which is explained in detail in Chapter 1. The control drive train has the following components:

- Four ACDs;
- One dSPACE unit: MicroAutoBox;
- Two PCBs setting connections between ACDs and motors;
- One converter;
- CAN bus;
- One laptop for HMI purpose;

Each wheel has one motor controller, sending control data to the MicroAutoBox which permits the drive to have total traction control from a laptop. Furthermore, the ACDs have their own CAN controller to receive and transmit signals. During the design process of the control drive train, it is really important to be careful about the location of the MicroAutoBox in the vehicle. Its hardware is of high cost, which should be away from the critical components of the vehicle. One is the battery pack, since it can be really dangerous in case of over temperature.

2.3 Electrical Components of the Drive Train

In this section the electrical components of the diagrams presented in Figure 2.2 and 2.3 are described in detail. Note that the battery was chosen and investigated by a team member.

2.3.1 In-wheel motor

In-wheel or wheel hub motors are dimensioned to be located inside of the wheel avoiding mechanical components and increasing the efficiency of the system. There is a large number of researchers carrying out improvements in different sort of in-wheel motors for direct drive applications. For further information, the following publications [9], [25], [12], and [23] investigates in detail different types of in-wheel motors, regarding their torque density.

In an wheel hub motor application, the rim should be prepared to handle large part of the vehicle body weight. In additional, its maximum torque is significantly dependent of the diameter, which should fulfill the requirements of the vehicle. The main characteristics of this sort of motors for drive applications are shown as follows [25]:

- High instant power and high power density;
- High torque at low speeds for starting and climbing, as well as high power at high speed for cruising;
- Very wide speed range including constant-torque and constant-power regions;
- Fast torque response;
- High efficiency over wide speed and torque ranges;
- High efficiency for regenerative braking;
- High reliability and robustness for various vehicle operating conditions;
- Reasonable cost.

Moreover, in-wheel motors increases the complexity of the suspension and steering systems due to the large value of the unsprung mass. Though, the ACM should be designed carefully in order to reduce the impact of this problem.

In-wheel Specification and Topology

Table 2.1 shows the in-wheel motor characteristics of the RCV 2013.

It is an air-cooled permanent magnet synchronous motor for low speed applications which can deliver high peak torque. The topology is based in a 3-phase system, outer

Table 2.1: In-wheel motor specification

In-wheel motor: PRA 230 - 48V DC	
Rated Output Power (kW)	1.8
Rated Output Torque (Nm)	33
Peak Output Torque (NM)	150
Rated Current (A)	42.10
Voltage AC (V)	33.30
Rated Speed (RPM)	520
Pole Number	32
Frequency (Hz)	138.67
Active Width (mm)	87.3
Diameter (mm)	255
Active weight (kg)	13.8

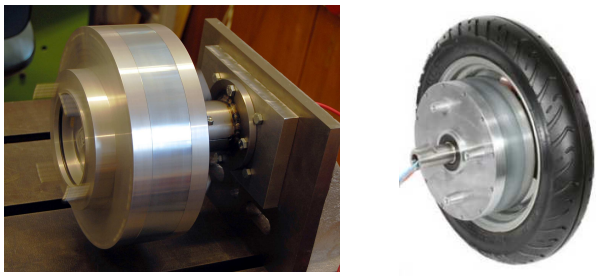

Figure 2.4: In-wheel motor of the RCV 2013 (PRA 230).

rotor, axial field, permanent magnets, and wheel hub motor. In each motor there is a rotary encoder of 8-bit resolution (AM256,RLS), which delivers position data in order to be possible to control the speed in a precise way. It offers the possibility to synchronize all the traction drive units of the electric drive train. Inside of the motor there is also one temperature sensor (P/N KTY 84-150 Philips) located on the critical parts of the stator winding. Hence, it can be monitored which able to prevent the demagnetization of the magnets and their destruction at high temperatures.

Figure 2.4 shows the in-wheel motor (PRA 230) of the RCV 2013 produced by Heinzmann Company.

2.3.2 Motor Controller (AC Drive)

The specification of each AC Drive is presented in table 2.2.

It has incorporated flux-vector control techniques offering high performance and efficiency. The logic and software, is appropriated for induction or brusheless PM motors. In this particular case, it was programable for the in-wheel motors PRA230. There is also a closed-loop speed regulator to maintain constant reference speed, and neutral-braking when stopped. Indeed, it was used torque control techniques, which is more appropriated

Table 2.2: Motor controllers specification.

Motor Controller: ACD 4805-P2	
Nominal DC Supply (V)	48
Voltage Range (V DC)	18-63
Driving Current (1 hour) (A rms)	75
Power output (1 hour) (kVA)	3.8
Driving Current (2 min.) (A rms)	200
Power output (2 min.) (kVA)	9.3
Switching Frequency (kHz)	8
Weight (kg)	1.6

to control each ACM separately.

The drive has the possibility to increase the speed in both directions, full four-quadrant is available. In additional, when braking regenerative energy is stored in the battery. CAN bus interface is the sort of communications for safety and readability of the system. Furthermore, the ACD 4805 has protection against under voltage, over voltage, over current and reverse polarity, and over temperature conditions. The motor controllers (ACD 4805) of the RCV 2013 is shown in Figure 2.5.

2.3.3 Battery Pack

The battery pack of the RCV was chosen based in the following criteria: lightweight, compacted, and hight density power per kilogram. Two topologies were discussed: the lead-acid battery and lithium-polymer cells battery. A common lead-acid battery has around 18kg with a capacity, for instance, of 40Ah and 12 V. In order to have the same capacity and DC voltage it is necessary to connect 3 lithium-polymer cells of 4.2V/40Ah in series, resulting in 12.6V and 3kg of weight. Regarding that, the suitable technology for the RCV is lithium-polymer cells of 4.2V/40Ah which can be seen in Figure 2.6.

The input voltage range of each ACD is between 18-63 V DC. Assuming that, 14 lithium-polymeer cells of 4.2V/40Ah were connected in series, which results in a total of 58.8V when fully charged. It is assumed to be necessary in average half of the total drive train power (3.6kW) corresponding a 75A required. As a matter of fact, for such power the battery will be discharged in approximately 32min. There are some restrictions concerning the upper and lower limit voltage of a lithium-polymeer cell when charging or discharging. In this case, it was used one Battery Management Unit (BMU) with the following characteristics:

- Maximum voltage of 4.25V per cell;
- Maximum discharge/charge current of 180A;
- Minimum voltage of 2.5V per cell;

Figure 2.5: Motor Controller (ACD 4805)

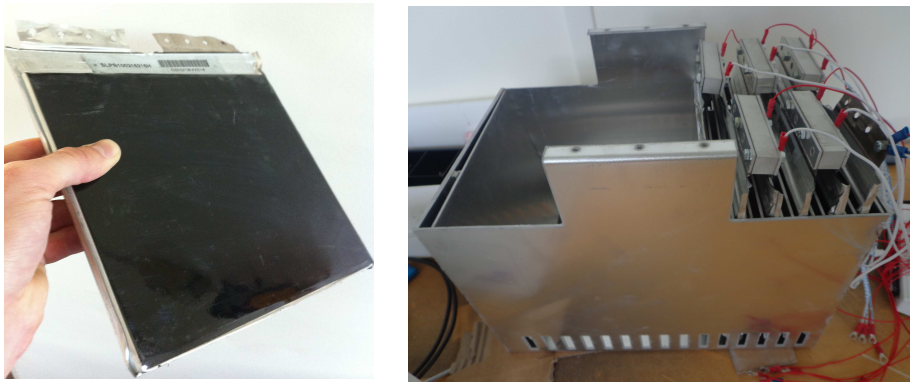

a) b)

Figure 2.6: a) Lithium-Polymer cells of 4.2V/40Ah; b) Battery pack (not completed);

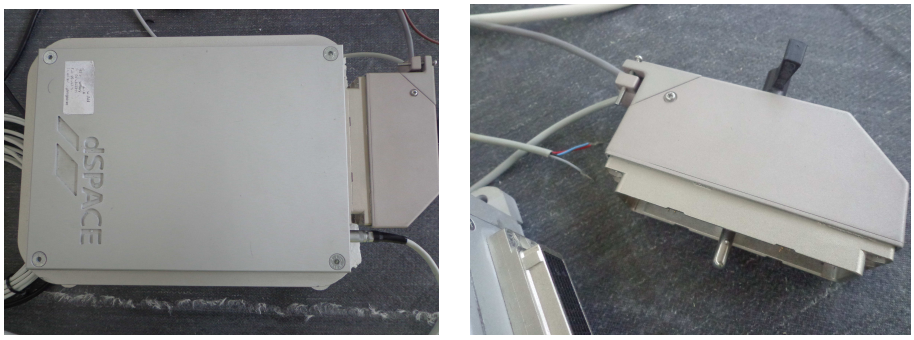

a) b)

Figure 2.7: a) MicroAutoBox 1401; b) ZIF connector;

- Temperature limit of 80 °C.

Based on the battery system presented, the battery pack is protected against short-circuits, over voltage, under voltage, and hight temperature. It is of great importance that the designer of the battery give additional attentions to the isolation of each cell against external conductive material, for instance, battery frame. Indeed, the cells will have extra protection against impacts when driving in warped roads or external strikes.

2.3.4 Master Controller

The master controller of the RCV is a dSPACE unit (MicroAutoBox 1401) with a variety of control options. The hardware is robust and compact being suitable for vehicles prototypes. It is a real-time system which can be operated by it self as an ECU or by laptop. Applications like chassis-control, body control, power train, and X-by-wire are the common ones [6].

The MicroAutoBox 1401 of the RCV is used as a CAN interface. The model to control all the drive train was build in Matlab/simulink by using the extension of Real-time interface CAN Blockset. The total control is done with a laptop using an interactive platform in dSPACE ControlDesk. In order to connect the MicroAutoBox to the laptop it is necessary DS821-34mm Link Board. Figure 2.7 shows the MicroAutoBox hardware and its ZIF connector. The ZIF connecter ensures all the I/O signals and power supply. All the I/O of the ZIF connector can be found on the help menu of matlab. For that, a license (dongle) is needed. The voltage supply of the MicroAutoBox 1401 is between 6 to 40V, which should not be exceeded.

2.3.5 DC/DC Converter

It is necessary one DC/DC converter step-down due to the low value of voltage of the contactor coils and MicroAutoBox. Figure 2.8 shows the key start diagram of the system.

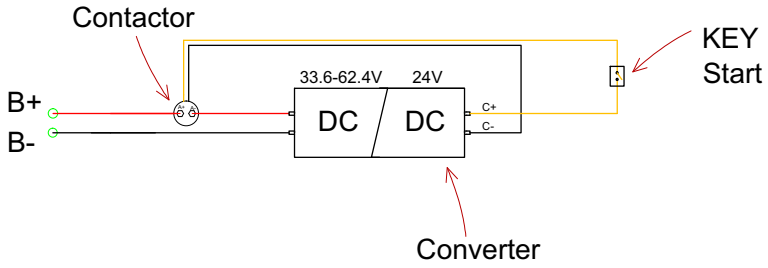

Figure 2.8: Key start diagram of the system

The system is turned on after supplying the required voltage of the contactor coils. A suitable DC/DC buck converter is the RSD-100C-24 available on Elfa. The input voltage is between 33.6-62.4V, and its output is 24V. The efficiency of the RSD-100C-24 is around 91% which is a reasonable value for low power converters (100 W) [19].

2.4 Initialization of the ACD

In this section, it will be shown how to initialize the CAN bus system. Furthermore, after doing the following instructions, the ACDs will be ready to receive and send PDOs or SDOs.

In order to make the ACDs operational, it is necessary to send an NMT message from the dSPACE unit to the ACD. The NMT start message consists of 2 bytes, byte 0 is the instruction code and byte 1 is the node address. The instruction code shall be 0x1h for NMT Start message and the node address 0x0h to reach all nodes. The COB-ID shall be set to 0x0h for NMT. After that, all the nodes are ready to receive and transmit messages. Indeed, the PDO traffic is activated and the ACDs expect to receive PDOs.

Table 2.3 shows an example of communication between the master device (dSPACE unit) and the slave (ACD 4805). First a NMT start message is sent, and after a SDO with index 2020h and sub index 0Ch is sent by the host. The SDO presented has the objective to activate the torque control mode instead of speed control mode of the ACD. For that, it is necessary to write the value of 3 on the parameter of the object dictionary with the respective index and sub index.

Table 2.3: Sample trace communication.

CAN ID	Data Length (bytes)	Message	Description
0x0	2	01 00	NMT start message
0x580	4	2F 2020 0C 03 00 00 00	SDO message

PDO messages could be sent after or before the SDO. Table 2.4 shows an example of a RPDO message. The COB-ID for RPDO is 0x200h + node ID and for TPDO is

0x180h + node ID.

Table 2.4: RPDO message 1 of the ACD 4805.

Byte	Index	subindex	Description
12	0x2000	1	Enable power stage
34	0x2000	2	Command Speed
5	0x2000	5	Command Acceleration
6	0x2000	6	Command Deceleration

2.5 dSPACE ControlDesk Interface

In this section, it is presented the interface created in dSPACE ControlDesk for the control of the RCV drive train during experimental evaluations. Figure 2.9 shows such ControlDesk interface.

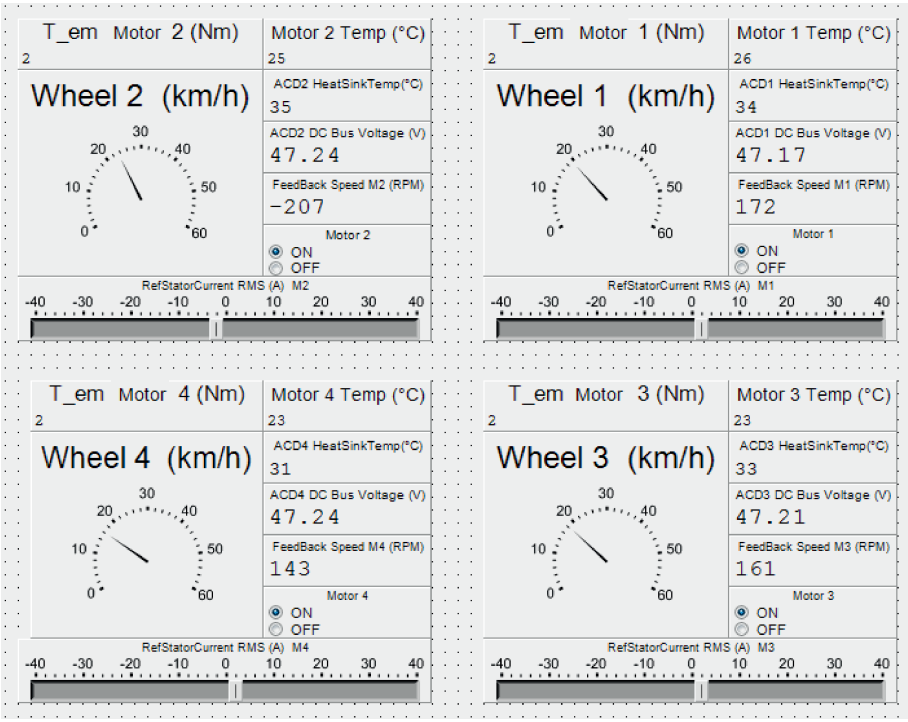

Figure 2.9: Control of four in-wheel motors using dSPACE ControlDesk.

This interface is constituted by four individual menus; each one monitors and controls one electrical machine. The motor is controlled by setting reference current, which is proportional to the torque. The motor stator windings temperature is constantly being measured in order to prevent fatal damage of the permanent magnets or other material.

The user is also able to observe the heat sink temperature of the converter, electromagnetic torque in each wheel, the DC-link voltage of each converter, and the speed in km/h and rpm. There is also, the possibility to turn off one or more electrical machines in case that the power of the battery is lower or even if one motor is broken.

2.6 Tuning PI controllers of the ACDs

The measurements results presented in this section have the objective to observe the current step response and the voltage limits of the ACDs 4805. The diagram of the control method (FOC) implemented in the ACDs can be seen in Figure 2.10. There is the possibility to change individually and directly the proportional and integral gains of the ACDs via CAN bus. First, the current controller of each ACD was tuned by setting a suitable proportional and integral gains. Figure 2.11 shows the current step response for a rise time of $2ms$. In this case, the overshoot is too high, around 85%, and it is necessary to decrease mainly the value of the integral gain. During this measurement, the motor was giving some noise when even at 0 speed. Such high overshoot, induce harmonics and decreases the quality of the wave current. Furthermore, the life time of the motor is decreased significantly. After several attempts, a rise time of $5ms$ was chosen. Figure 2.12 shows the results obtained with a load of $12A$. In this case, the overshoot is much lower than with a rise time of $2ms$. Furthermore, it can be improved but for this application it is acceptable.

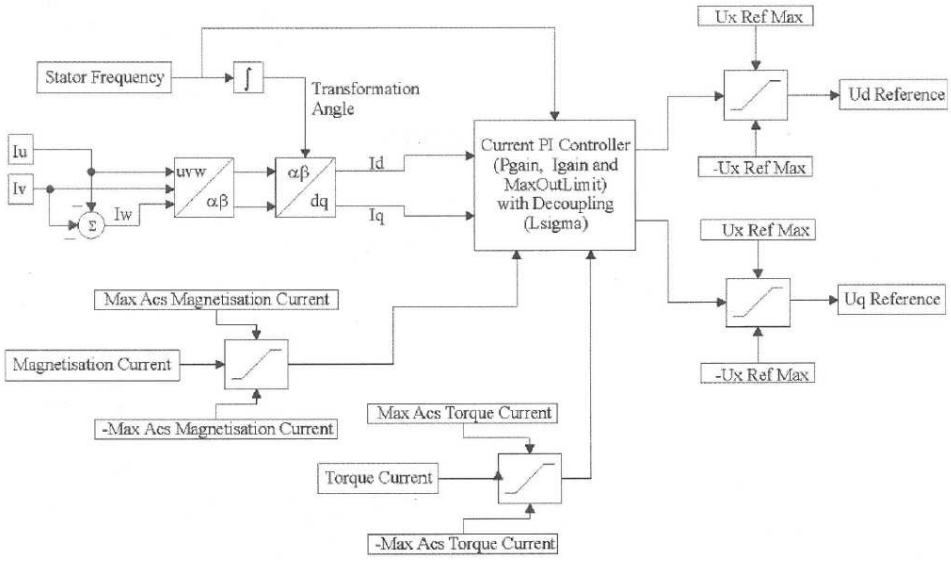

Figure 2.10: Control diagram of the ACDs.

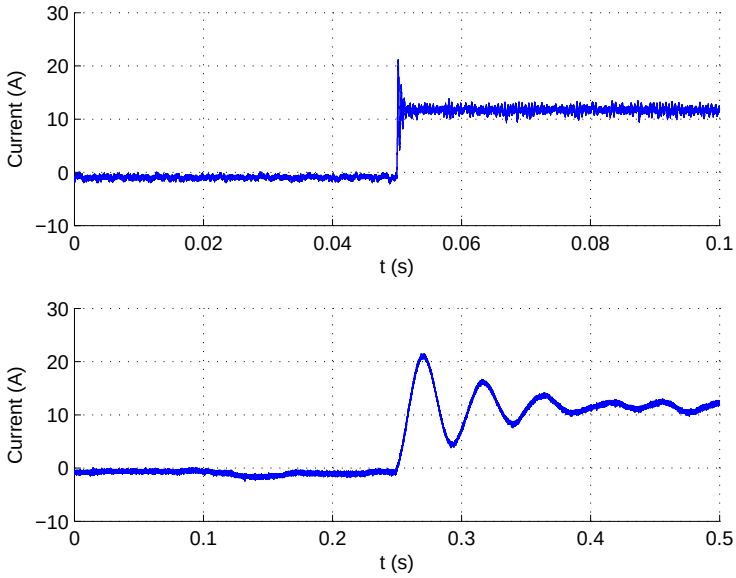

Figure 2.11: Current step response with rise time of $2ms$.

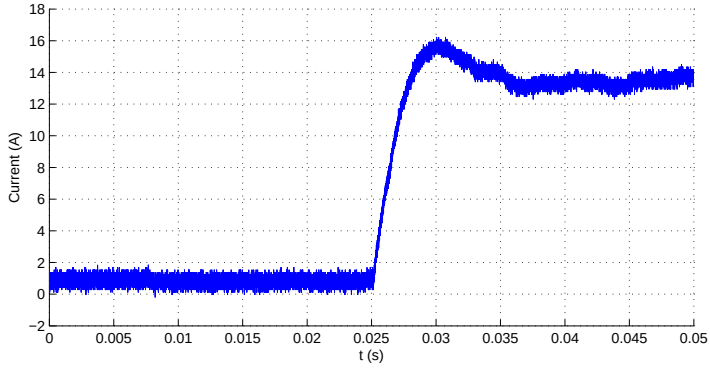

Figure 2.12: Current step response with rise time of $5ms$.

Voltage Limit of the ACDs

The limit of the stator voltage of an inverter-fed PMSM is given by equation 1.23. The ACDs (4805) with a DC-link voltage equal to $48V$ were not capable to provide enough power to obtain the rated torque provided by the motor (PRA 230). Figure 2.13 shows the maximum phase-to-phase PWM waveform supplied to the motor, which corresponds a limited torque equal to $16Nm$ at rated speed. In order to obtained the rated torque it is necessary to increase the DC-link voltage to $55V$. Figure 2.14 shows the stator phase-to-phase PWM waveform at rated torque and speed.

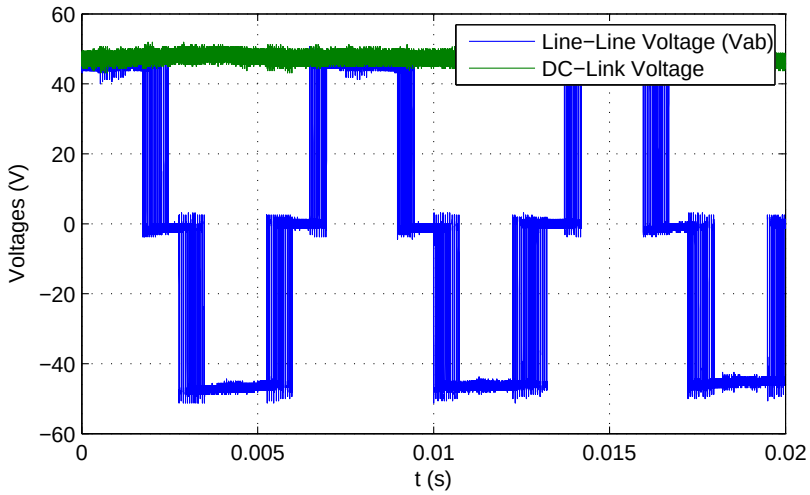

Figure 2.13: Saturated PWM Waveform at 48 DC-link

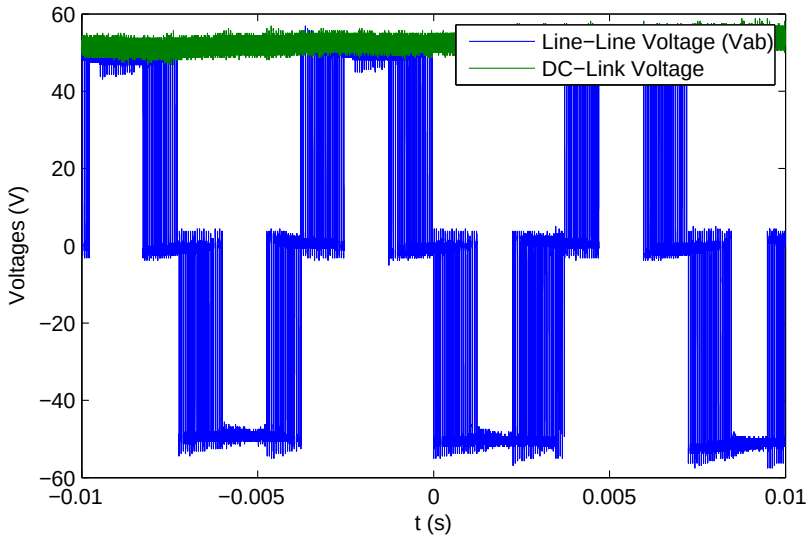

Figure 2.14: completely saturated PWM Waveform at 55V DC-link

2.7 Summary of the Chapter

In this chapter a new electric drive train concept was presented, pointing out the characteristics of each component and some relevant information about it. The main idea was based in a flexible, innovative, and relatively high efficiency architecture being possible further research. The control concept is based in a single CAN bus connected to the CAN controllers of each ACD and MicroAutoBox. Moreover, it should be avoid magnetic interferences between signal and power cables, and devices.

In the second part, the initialization of the PDO and SDO traffic between the master controller and the slaves was explained with an example. After, detailed information shows how to tune the PI controllers of the ACDs. Finally, the dSPACE ControlDesk interface used to communicate between devices is presented.

Chapter 3

Heat Sink of Semiconductors

Microelectronics, for instance diodes and transistors, produces a large amount of heat when operating at high power. In order to prevent the over temperature and the destruction of these switching devices, it is necessary to build an optimized and appropriated heat-sink. Furthermore, the power dissipation increases mainly with the internal temperature, and the losses become extremely high at temperatures of $200°C$ [14]. From manufactures, typically the maximum junction temperature is often $150°C$ which depends on the different parameters of each device, for instance: on-state condition voltages, switching times and switching losses. However, one of the most important input parameters in the design process, is the expected worst-case junction temperature, typically below $120°C$ (worst-case design input).

There are devices which can operate at temperatures above $200°C$. In this case, the device life time is short, and its performance is lower than the devices with maximum junction temperature equal to $120°C$ [19]. During the heat sink design, the designer should have in consideration the environment of the application, size and weight of the heat sink, location of the material, and surrounding temperature. If the heat sink is built to be natural convention, its fins should be mounted in vertical position to facilitate the circulation of the air. Indeed, the designer should choose the appropriated cooling system which can be: by natural convention, by a fan, or the use of liquid cooling.

There are different possibilities to remove heat from the heat sinks. These methods are characterized by the cooling system installed. The common heat sink categories used in converters are described bellow [13]:

- **Passive Heat Sinks** are appropriated for natural convection applications. The Heat sink dissipation does not rely on the designed supply of air flows.

- **Semi-Active Heat Sinks** leverage off existing fans in the system.

- **Active Heat Sinks** employ designated fans for its own use, such as fan heat sinks in either impingement or vertical flows.

- **Liquid Cooled Cold Plates** are based in tubes or similar, acrossing the heat sink, with use of pumped water, oil, or other liquids.

3.1 Thermal Equations

There are three possibilities for heat transfer on converters: conduction, convection and radiation. In most all of the cases the heat is transferred by conduction. If the cooling system uses liquids or gases the heat is transferred by convection. Radiation heat transferring is based on electromagnetic waves. The basic equation for thermal flow is given by equation 3.1.

$$Q = \frac{\Delta T}{R} \tag{3.1}$$

where Q is the rate of transfer heat between two parts (W), ΔT is the temperature gradient, and R is the thermal resistance. For conduction heat transfer, the rate of transferred heat (energy flow per unit time) can be obtained by equation 3.2 [14].

$$q_c = -kA\frac{\Delta T}{d} \tag{3.2}$$

where A is the cross-section area, d is the heat sink length, and k is the thermal conductivity. Typically heat sinks are made of 90% of pure aluminium. In this case the thermal conductivity is $220\ W.m^{-1}.^{\circ}C^{-1}$.

Heat transferred by convection can be forced or natural type. In natural type, the movement of the fluid is done by its density. Forced convection is based on the use of fans or pumps for movement of the fluid. Heat transferring by convection is given as follows [2]:

$$q_h = hA(T_1 - T_2) \tag{3.3}$$

where h is the convection heat transferred coefficient ($W.m^{-1}.^{\circ}C^{-1}$), and $T_1 - T_2$ is the temperature gradient between the surface of the solid material and the nearest layer of fluid.

Heat transfer via radiation is given by the Stefan-Boltzmann law, and it can be seen in equation 3.4 [14].

$$q_r = 5.7 \times 10^{-8} EA(T_s^4 - T_a^4) \tag{3.4}$$

where E is the emissivity of the surface, T_s is the surface temperature, T_a is the ambient temperature, and A is the outer surface area of the heat sink.

3.2 Thermal Resistance in Heat Sinks

The configuration of thermal resistances in a semiconductor can be seen in Figure 3.1. It is important to keep the junction temperature within reasonable bounds, which should be as low as possible. The thermal resistance junction-case ($R_{\theta jc}$), which is between the interior of the semiconductor and the outside of the case enclosing the device, is minimized by the manufacturer. This value is usually given on the data sheet of the device. The device user should design an appropriated heat conduction path between the case and the ambient. This path is constituted by the enclose of two materials: thermal grease, and the heat sink. The thermal grease defines the thermal resistance between the case and the heat sink ($R_{\theta cs}$). The heat sink can be easily found by a variety of providers. There are available a variety of aluminium heat sinks of different shapes for cooling the device.

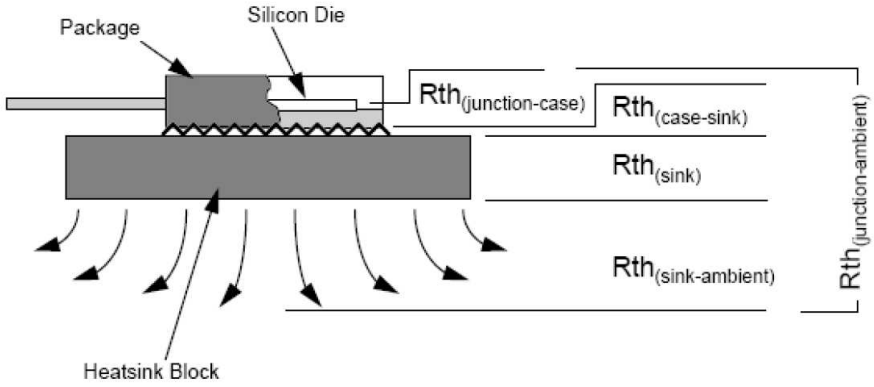

Figure 3.1: Configuration of several thermal resistances in a semiconductor.

Heat Sinks cooled by natural convection, should have space between their fins and at leat 10 to $15mm$ [14]. Furthermore, a coating of black oxide covering the heat sink reduces the thermal resistance about 25%, but it increases the cost. Adding a fan, the thermal resistance of the heat sink decreases significantly, and it can be made smaller and lighter. In higher power ratings, force-cooled heat sinks should be used.

The device user should choose the heat sink based on the maximum junction temperature of the device. First, a worst-case design is specified. From equation 3.5, the allowable maximum junction-to-ambient thermal resistance can be obtained.

$$R_{\theta ja} = \frac{T_{j,max} - T_{a,max}}{P_{Loss}} \tag{3.5}$$

where $T_{j,max}$ is the maximum junction temperature, $T_{a,max}$ the maximum ambient temperature, and P_{Loss} is the sum of on-state losses and the average switching losses. The total thermal resistance of a semiconductor from junction to ambient is given by equation

3.6.

$$R_{\theta ja} = R_{\theta jc} + R_{\theta cs} + R_{\theta sa} \tag{3.6}$$

The resulting junction temperature is

$$T_j = P_d(R_{\theta jc} + R_{\theta cs} + R_{\theta sa}) + T_a \tag{3.7}$$

where P_d is the power dissipation, $R_{\theta sa}$ the sink-ambient thermal resistance. and T_a is the ambient temperature.

In heat sinks the heat is transferred by convection and radiation. Meanwhile, the total thermal resistance $R_{\theta sa}$ comprises both convection and radiation resistances. From equations 3.3 and 3.4 such thermal resistances are obtained.

$$R_{\theta sa,con} = \frac{1}{hA} = \frac{0.13}{A} \quad (^\circ C/W) \tag{3.8}$$

$$R_{\theta sa,rad} = \frac{1}{5.7 \times 10^{-8} EA(T_s + T_a)(T_s^2 + T_a^2)} \tag{3.9}$$

3.3 AC Drive Heat Sink

The heat sink of the motor controller (ACD 4805) was chosen considering the specification presented in table 3.1. The switching losses of the inverter at $8kHz$ were obtained from Figure 3.2. The heat sink thermal resistance was estimated by using equation 3.6 and 3.7. It results in a thermal resistance equal to $0.2818\ ^\circ C/W$. In this case the device user should buy a heat sink with a thermal resistance below or equal to $0.3\ ^\circ C/W$. The heat sink length and width were obtained from the ACD dimensions, which are $150 \times 200\,mm$. A reasonable value for the heat sink height is equal to $63\,mm$. Figure 3.3 shows an appropriated heat sink material with thermal resistance equal to $0.3\ ^\circ C/W$. From the thermal model presented in equation 3.7, it results a junction temperature of $102^\circ C)$ by assuming the converter power losses equal to $110W$ and ambient temperature of $25^\circ C)$.

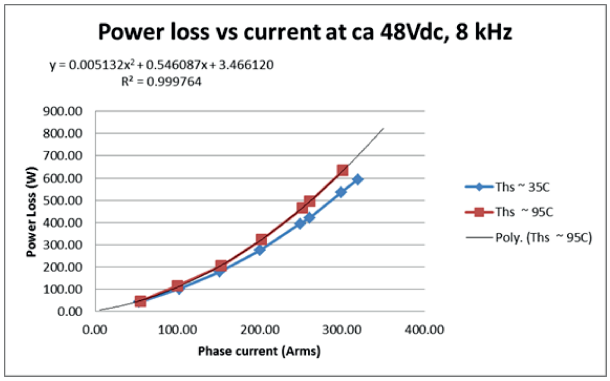

Figure 3.2: Inverter switching losses in function of current at $8kHz$

Table 3.1: Design input parameters of the heat sink.

Heat Sink Specifications	
Maximum junction temperature ($^{\circ}C$)	125
Maximum ambient temperature ($^{\circ}C$)	50
Maximum current(A)	100
Junction to case thermal resistance ($^{\circ}C)/W$	0.1
Case to sink thermal resistance ($^{\circ}C/W$)	0.3
Switching losses (W)	105
On-state losses (W)	5

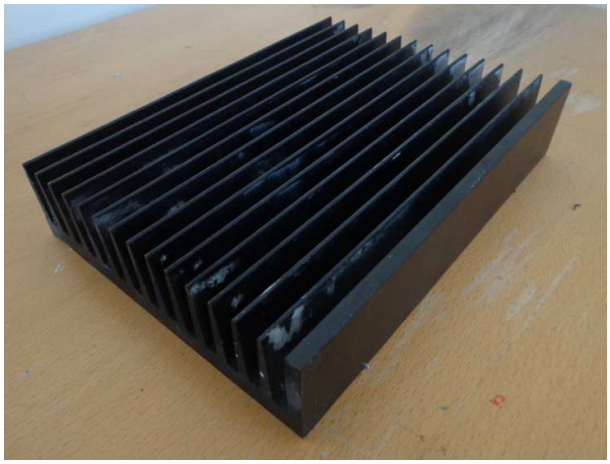

Figure 3.3: ACD 4805 heat sink.

3.4 Experimental Results

In order to evaluate the thermal model presented above, the ACD (4805) case and motor (PRA 230) temperature was observed at two different loads. First, measurements were done at rated torque ($33Nm$), which can be seen in Figure 3.4. After, the torque of the motor was increased to $40Nm$ and the speed decreased to $300rpm$, which is presented in Figure 3.5. The environment, where the measurements were done, can be considered the worst case due to the fact that was a closed room without ventilation.

From the device manufacturer, the case temperature should not be higher than $125^{\circ}C$. It can be seen, in these both critical cases that the case temperature were $53^{\circ}C$ and $64^{\circ}C$ which are below the limit. From the thermal model presented in equation 3.7, the estimated steady state junction temperature at rated torque ($33Nm$) was equal to $54.4^{\circ}C$. Comparing both results ($53^{\circ}C$ and $54.4^{\circ}C$) it shows that the thermal model is approved and there is no need for a heat sink with force convection or other cooling system more sophisticated.

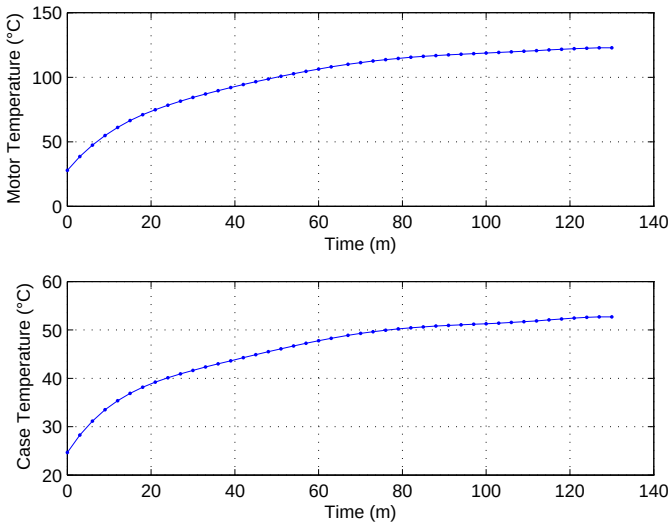

Figure 3.4: Motor and ACD case temperature at rated torque and speed.

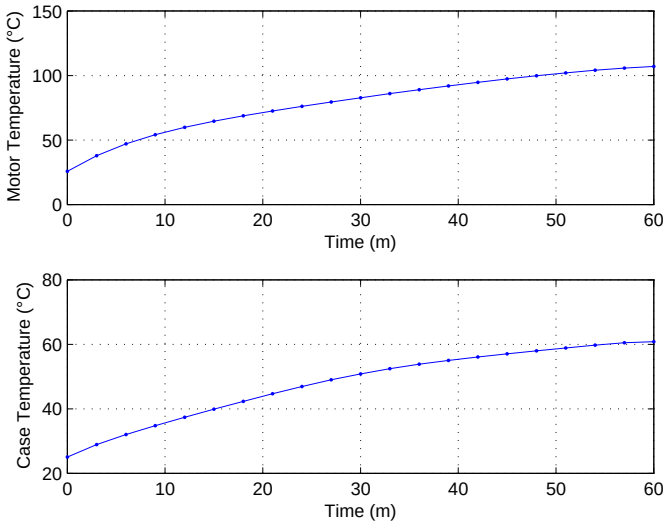

Figure 3.5: Motor and ACD case temperature at 40Nm and 300rpm.

3.5 Summary of the Chapter

In this chapter, the heat sinks of the ACDs are studied and evaluated. First, thermal equations and thermal resistances of the combined inverter and heat sink, were developed and discussed. Second part of the chapter, the experimental results shows that the heat sink chosen by the device user was appropriated and effective. The temperature of the motor

during 130 minutes achieved $123°C$ at rated torque and speed, which was quite critical. The magnets are sensible to the temperature, and above $120°C$ there is a high possibility of demagnetization. However, the battery pack is only able to provide rated power during about 15 minutes, and from Figure 3.4 it achieved $64°C$ when operating during such time. For the worst case scenario, results shows that the motor and ACD operates safely and mainly for a short period of time (lesser 100 minutes) at rated torque and speed.

Chapter 4

Motor Efficiency

In this chapter, the efficiency of an in-wheel motor is presented and discussed. Also, the efficiency of the motor controller is shown and analyzed.

4.1 Motor Efficiency (PRA 230)

The setup diagram used to obtain all measurements is shown in Figure 4.1.

The average power, frequency, current, voltage, and other relevant variables were measured in different places of the setup. Therefore, the speed controlled machine was working has a generator and the torque controlled machine has a motor. Both AC Drives were configured based on the type of motor control (speed or torque). The machine to be investigated in detail is the motor due to the use of torque control mode (FOC) in the electric drive train of the RCV. Figure 4.2 shows the experimental setup with both machines coupled.

In this method, the motor power losses are estimated according to:

$$P_{loss} = \frac{P_1 - P_2}{2} \tag{4.1}$$

where P_1 is the input power of the motor, and P_2 is the output power of the generator. The mechanical torque can be estimated as

$$T_m = \frac{P_1 - P_{loss}}{\omega_r} \tag{4.2}$$

Finally the efficiency of the motor can be estimated as follows:

$$\eta_m = \frac{P_1 - P_{loss}}{P_1} \tag{4.3}$$

The motor controller efficiency was estimated according with equation 4.4.

$$\eta_{acd} = \frac{P_{acd1} - P_1}{P_{acd1}} \tag{4.4}$$

where P_{acd1} is the input power of the motor controller, and P_1 the output power.

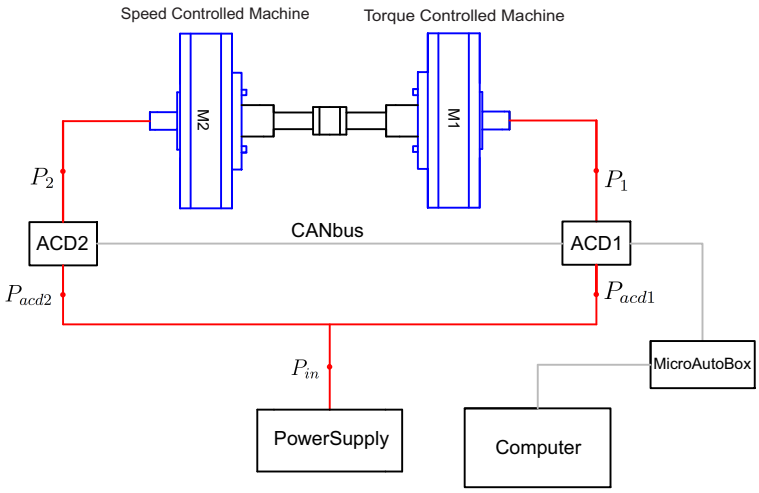

Figure 4.1: Diagram of the 2 in-wheel motors setup.

a) b)

Figure 4.2: a) Experimental setup; b)Two in-wheel motors coupled;

4.1.1 Back EMF and torque measurements

In order to calculate the electromagnetic torque of the motor it is necessary to estimate the magnetic flux. Meanwhile, figure 4.3 shows the BEMF measured at 520rpm. However, the phasor of the induced voltage per phase is obtained by computing the discrete fourier transform of the signal V_{ab} observed in Figure 4.3. The fundamental value of the induced voltage (phase to phase) obtained at rated speed is equal to $43.89V$. Furthermore, the magnet flux was calculated by using equation 1.7, which is $0.0290Wb$.

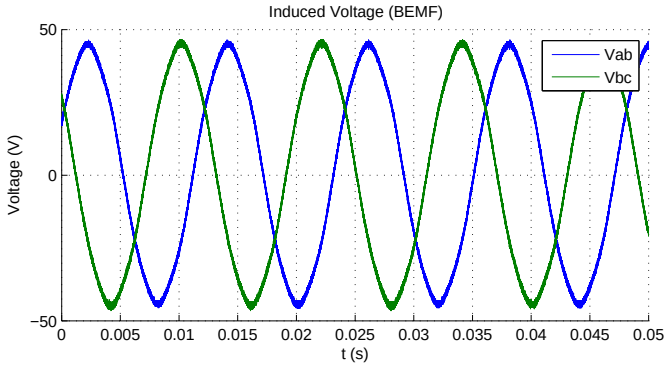

Figure 4.3: Induced voltage in the stator windings.

From the magnet flux obtained it is possible to calculate the electromagnetic torque for such respective load. Figure 4.4 shows the motor current at rated torque and its spectrum.

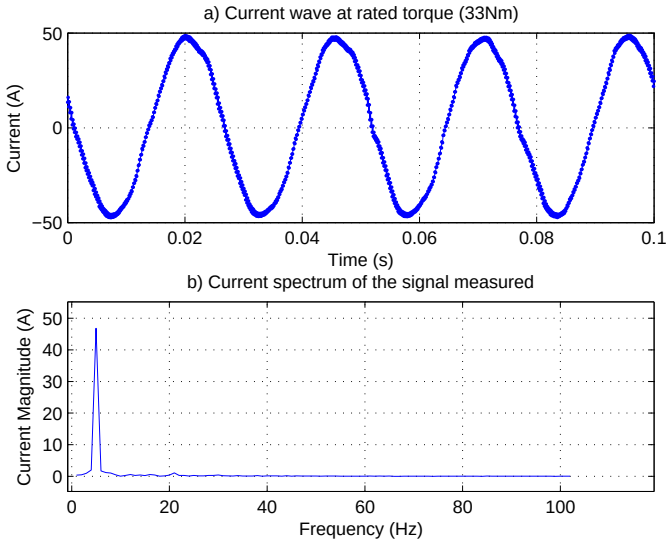

Figure 4.4: Current wave and respective spectrum at rated torque and 150 rpm.

Efficiency

The motor (PRA 230) efficiency was computed by using the method presented on the beginning of the current chapter. This method is based on data collected from measurements at different loads and speeds. Furthermore it was collected from the vehicle CAN bus, and from the power analyzers situated in each point ($P_1, P_2, P_{acd1}, P_{acd2},$ and P_{in}), which is shown in the diagram 4.2. Moreover, auxiliary tools where used to monitor the safety of the setup during measurements. Figure 4.5 shows the efficiency surface map obtained.

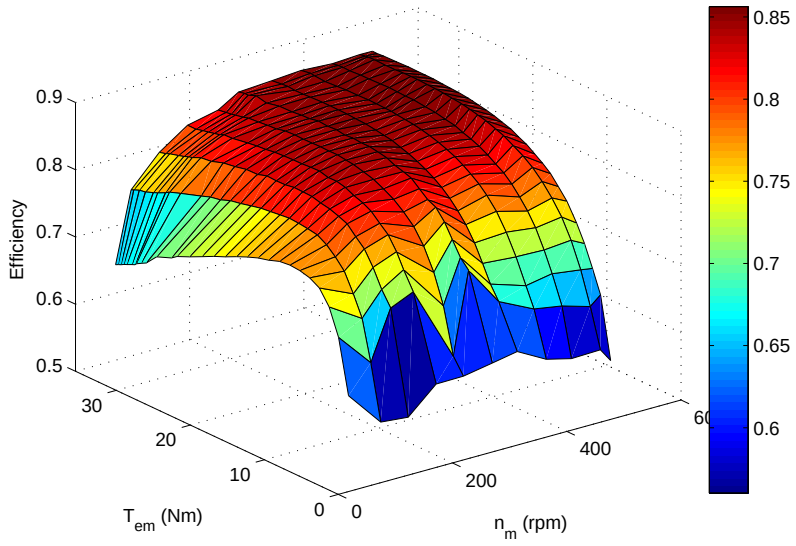

Figure 4.5: Motor efficiency map.

The figure above has 319 measurements of the active power, and each one is the average value of 64 periods. However, during measurements the oscillations of the active power were reduced significantly by taking the average value. The estimated efficiency obtained at rated speed and torque (33Nm and 520rpm) is equal to 85.55%. This value can be considered reasonable, due to the fact that the motor iron losses, the stator winding losses, and the friction losses were considered when estimating the efficiency. It is important to know that this value is an estimation and not the exactly efficiency of the motor. Indeed, the motor copper losses should be higher than the generator copper losses; for instance, during measurements it was observed that the stator winding temperature of the motor was higher than the generator. Meanwhile, in this method to estimate the efficiency, it is assumed that the motor losses are equal to the generator losses.

Also, the efficiency of the motor controller was estimated for the same speeds and loads. The results are shown in figure 4.6. At rated speed and torque the efficiency estimated is equal to 94.4%. This value is reliable and it is according with the efficiency pointed out

by the manufactures of the ACD (95%).

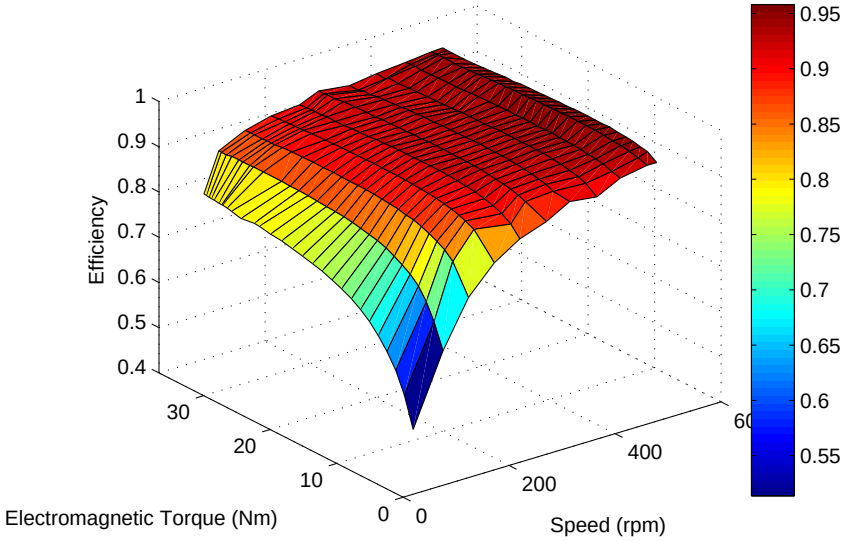

Figure 4.6: Motor controller efficiency map.

4.2 Summary of the Chapter

In this chapter, a possible method to estimate the motor and the ACD efficiency was presented. In the first part, it is described the equations used to estimate such efficiency. Also, the proposed solution to obtain the magnet flux of a PMSM are described, and it is based on measuring the phase to phase voltage of the stator. Such value is needed to estimate the electromagnetic torque. In the second part of the chapter, the results obtained to estimate the efficiency of a PMSM (PRA 230) and AC Drive (4805) are presented. The main conclusion of this chapter is that the motor efficiency can be estimated by a simple method, and such values can be trustable.

Chapter 5

Conclusions and Further Work

5.1 Conclusions

In this thesis, an electric drive train for the Research Concept Vehicle 2013 has been studied. The focus has been put on machines, motor controllers, and communication system. However, the results shows that this technology is reliable, safe, and promising.

The detailed description of the electric drive train components presented shows how this architecture works. It is based in a flexible, innovative, and relatively high efficiency system. However, during the installation of the system it is of great importance to avoid magnetic interferences between signal and power cables, and devices. Indeed, in-wheel motors, AC Drives, dSPACE unit, and the battery system are the most important components of the electric drive train, and it should be given major attentions when designing such drive train.

The control theory behind the motor controllers is based on field-oriented control. Meanwhile, a model was developed in Matlab/Simulink in order to observe its main principle. Simulations shows that it is important to avoid, if possible, PWM over modulation. PWM over modulation decreases the maximum torque available on the motor shaft. Moreover, possible solutions are: increasing the DC-link voltage of the converters, or implementation of field-weakening control strategies. Regarding the control implemented in the motor controllers, measurements shows different current overshoots when setting different possibilities for the proportional and integral gains. A rise time of $2ms$ originates a current overshoot of around 85% which was too high. Indeed, it was conclude that the PI gains of the controller should be set to have a rise time equal to $5ms$. Such current overshoot (approximate 20%) was considered acceptable for respective application.

To protect the motor controllers against over temperature it was necessary to design an appropriated heat sink. First it was assumed heat sinks based in natural convection. After obtaining the respective heat sink thermal resistance and material, measurements shows that natural convection was capable of cooling the converter.

In addition, a possible method to estimate the motor and AC Drive efficiency was

presented. Measurements have shown that the motor efficiency obtained is equal to 85.55% at rated torque and speed (33Nm and 520rpm). Such result are reliable due to the fact that the iron losses, copper losses, and friction losses were considered when estimating the efficiency map. Also, it was observed that the motor efficiency increases with the motor torque, and starts decreasing after some torque value. Regarding the efficiency of the motor controllers, results shows that it is possible to have a relatively high efficient controller (94.4% at rated torque and speed).

5.2 Further work

For the proposed motor controllers, implementation of field weakening control would be an interesting matter to be observed and analyzed. A drive train model in Matlab/Simulink in order to simulate and observe different drive cycles can be a topic of interest. Also, the study of an electric drive train with synchronous reluctance motors (SynRM) could be a promising technology due to the high torque available from such machines.

Appendix A

Drive train Connections of the RCV 2013

In this section, a guide for the electric drive train system of the RCV 2013 is presented. It is helpful information for those who may continue with the project. Meanwhile, it is important to read chapter 2 before starting it. Resuming, the guide will help the user to build the electric drive train with the diagrams presented in Figure A.1 and A.2.

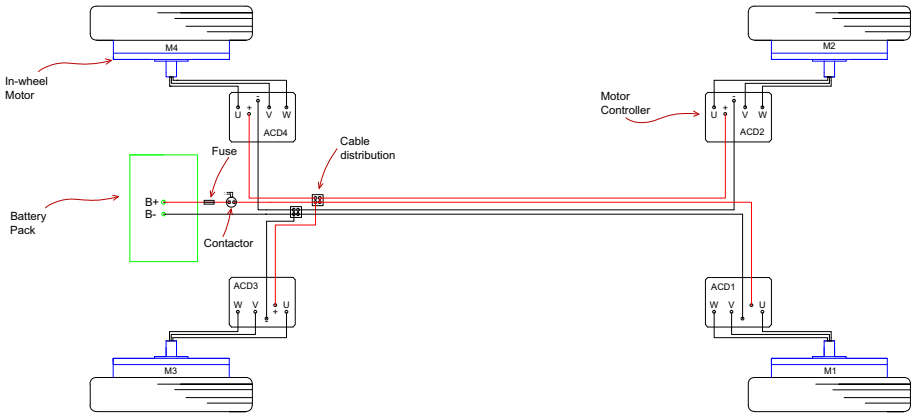

Figure A.1: Power drive train system of the RCV 2013.

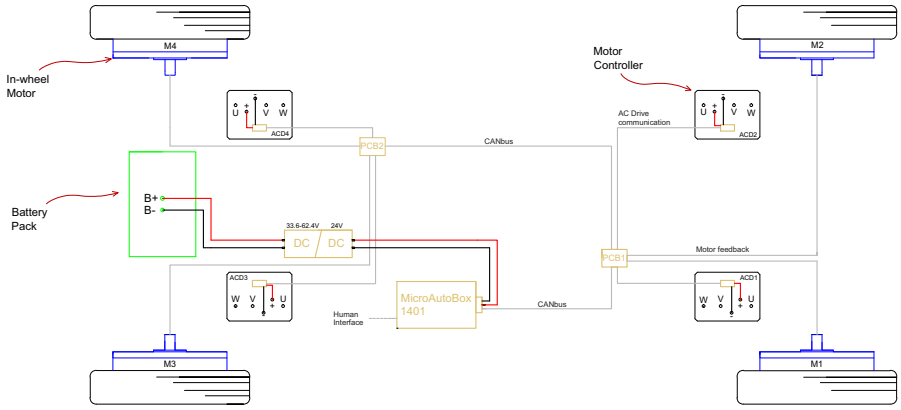

Figure A.2: Control cabling and electronic units of the RCV 2013.

First step - Equipment

First of all, the main equipment presented in chapter 2 should be collected. After that, each motor has their own controller (ACD 4805), and the user should find out which controller belongs to each motor. There is a number on the board characteristics of the ACD written by a marker, and there is another number in one side of the motor. For instance, motor 1 should be connected with ACD 1. This is due to the fact that the sensor position of the motor was calibrated by its own ACD. If the ACDs and motors are not ”married”, the motor will not run properly when sending reference torque.

Second step - Diagram connections

After collecting the main equipment and ”marring” the motors to the controllers, the user should be familiarized with the diagram connection of the ACDs 4805. Figure A.3 shows the diagram connections of each ACD. For further information the user should obtain the ACD documents (connection diagram, setting-up, and the user manual) provided by Heinzmann companies. Indeed, all the cables should be connected correctly to the ACD socket according with Figure A.3. There is already a connector with a cable (Connector 23p AMP seal) for each ACD, and two PCBs (Printed circuit board) for the respective connections between the motors, ACDs, CAN bus, and input power. ACD 1 and 2 should be connected to PCB 1. The schematics of the PCBs are presented in Figures A.4 and A.5. Note that each ACD has a CAN identifier (1 to 4) in order to be able individual control of the motors. Table A.6 shows the respective CAN IDs available for the ACDs. The ACD 1 has the CAN ID 0,..., and the ACD 4 has the CAN ID 3. At this stage, the user should be able to connect the motors to the respective ACDs. Note that the location of each motor on the chassis of the vehicle should be according with Figure A.1.

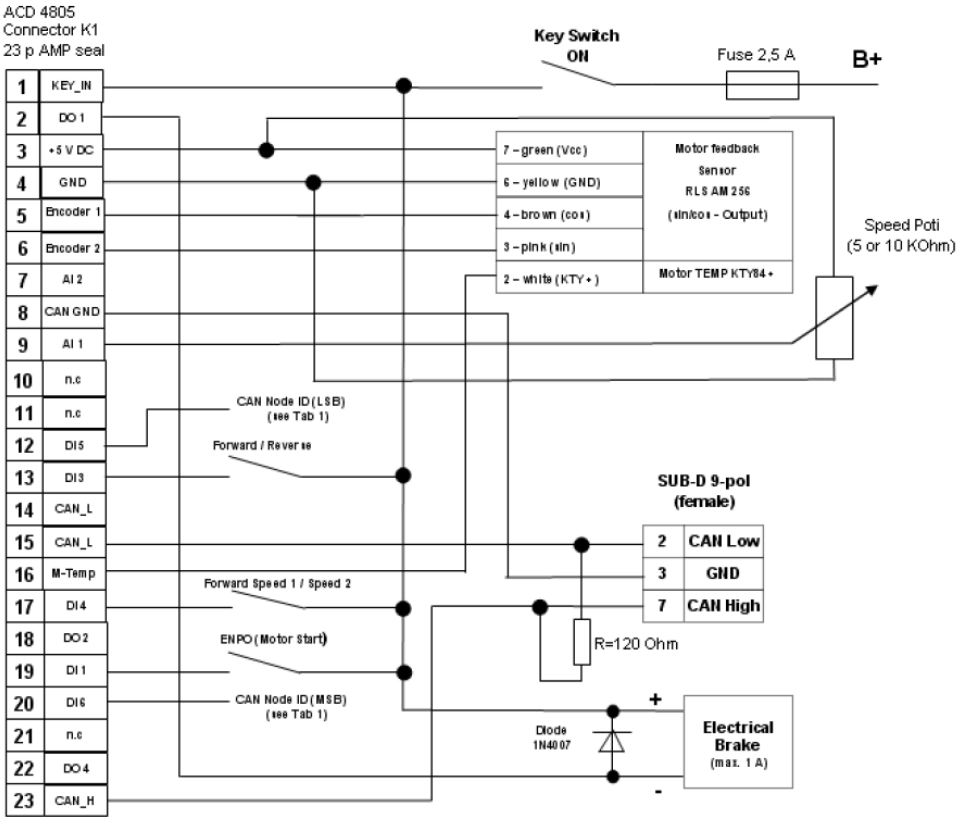

Figure A.3: Connection diagram of the ACD.

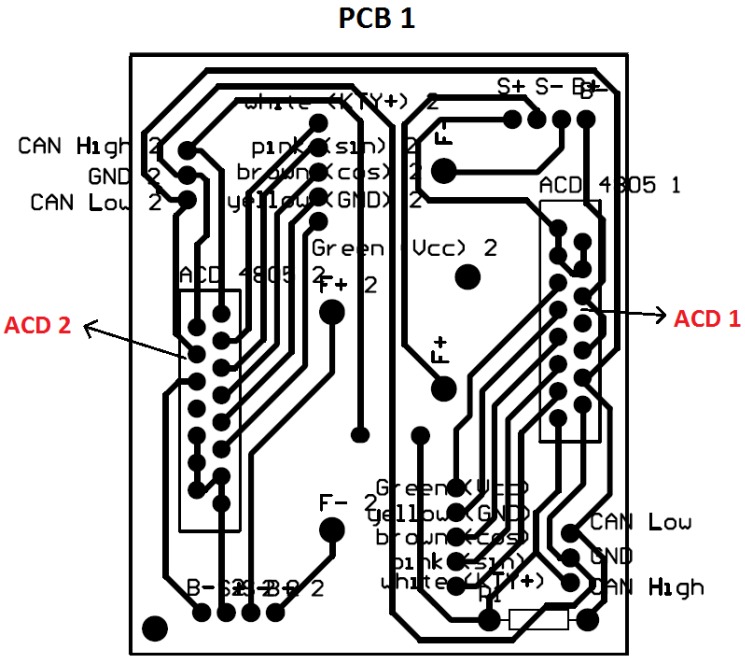

Figure A.4: Schematic of the PCW1.

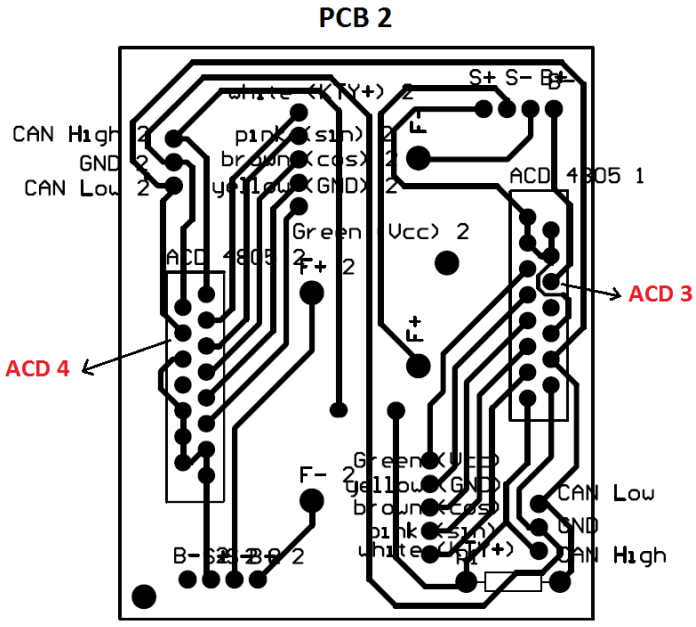

Figure A.5: Schematic of the PCW2.

CAN Node ID	Hardware ID	Connect Controller PIN 12 (DI5) to:	Connect Controller PIN 20 (DI6) to:
5	0	Battery–	Battery–
6	1	Key Input (PIN 1)	Battery– (B–)
7	2	Battery– (B–)	Key Input (PIN 1)
8	3	Key Input (PIN 1)	Key Input (PIN 1)
5	0	No connection	No connection

Figure A.6: CAN Node Addresses of the ACDs.

Important: The connector of each ACDs should be connected on the respective socket of the PCB, in other case it will not work properly. Also the placement of the motors on the chassis have to be correct, in other case the motors wont be synchronized.

Third step - CAN bus

After connecting correctly the connectors 23p AMP seal from the ACDs to the PCBs, the user should connect a CAN bus cable between both PCBs. From the schematic presented in figure **??** or **??** the CAN bus cable can be connected in one of the two CAN sockets (each socket has 3 pins: CANH, CANL, and GND) of each PCB. Furthermore, 48 volts should be supplied for each ACD. Meanwhile, in each PCB there 2 pins (B+, and B-) for the ACDs, and it has to be connected to the battery. Figure A.7 shows the connections to be done. Also, the sensor position of each motor have to be connected to the respective socket of the PCBs.

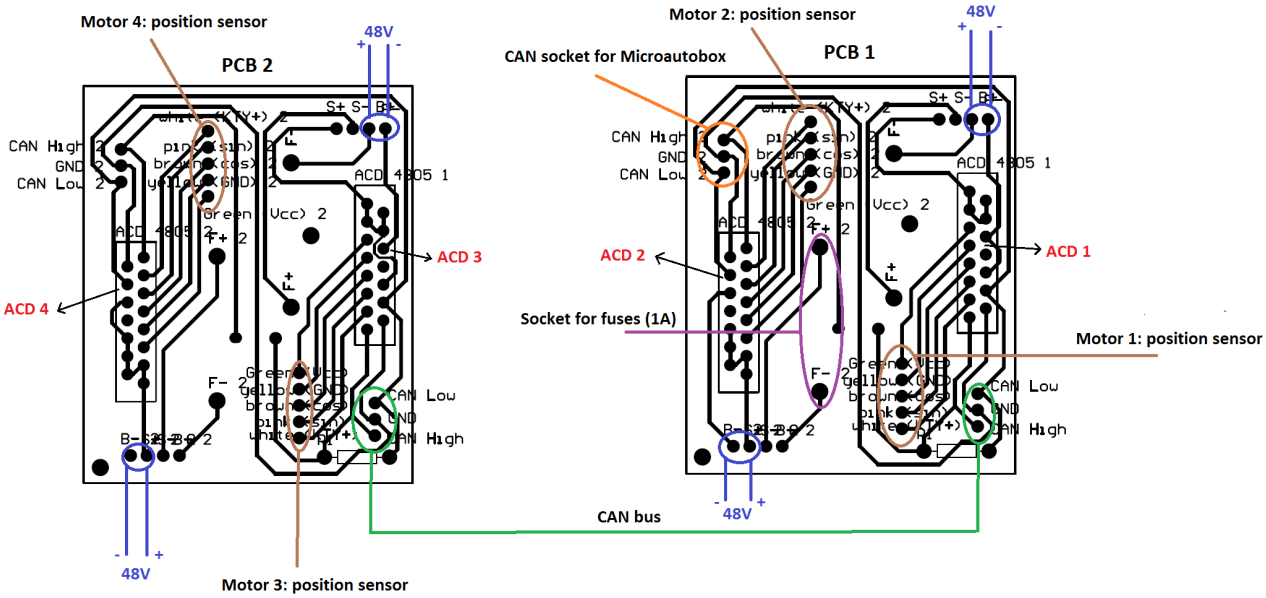

Figure A.7: CAN Node Addresses of the ACDs.

Fourth step - dSPACE unit: MicroAutoBox 1401

In this step, it is necessary to supply power to the microautobox. Also, the microautobox should be connected to the CAN bus. All the necessary cables for the microautobox are already plugged on the ZIF connector (Figure A.8). Note that the voltage input of the microautobox should not exceed 40 V, which implies the use of an DC/DC converter or a power supply with adjust of voltage.

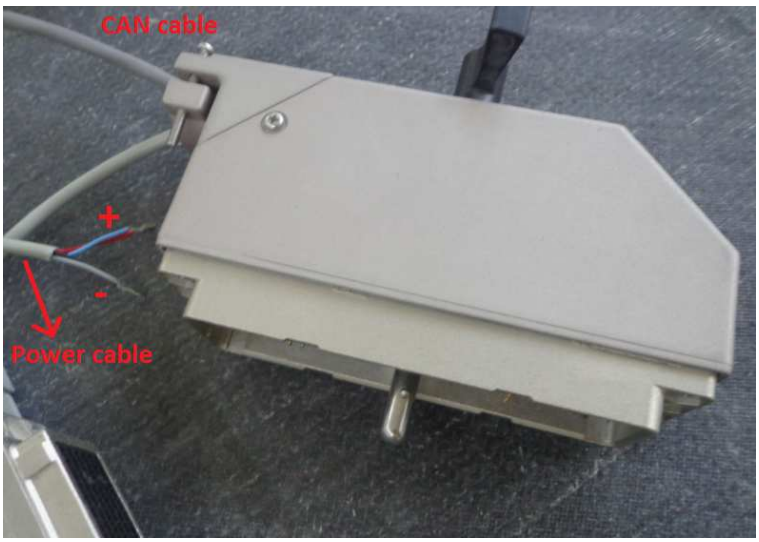

Figure A.8: ZIF connector of the Microautobox.

Last step - Initialization

At this stage all the control cabling of the drive train system have to be connected according to the diagram presented in Figure A.2. If yes, the user should connect the power cables for each equipment according to the diagram presented in Figure A.1, and maintaining the contactor in mode off (0 volts supplied the coils). Now, it is time to connect the microautobox to the laptop and to open the project ”Electric DriveTrain RCV v1.0: Experiment001” in ControlDesk NextGeneration. After, the contactor can be turned on (24V supplied to the coils). If everything was connected correctly, the information led of each ACD should be not blinking. However, at this stage the user can run the program in ControlDesk and control individually each motor. If it is blinking, there is probably a wrong connection on the setup. In case of an error during operation (for instance over speed of the motors), the system should be restarted.

Appendix B

List of symbols, subscripts and abbreviations

Symbols

A	cross-section area
B_m	viscous friction coefficient
d	heat sink length
E	emissivity of the surface
h	convection heat transferred coefficient
i_d	direct stator current component
i_q	quadrature stator current component
i_s	stator current
i_{smax}	maximum stator current
J_L	load inertia
J_M	motor inertia,
k	thermal conductivity
$k_{i,d}$	direct component of the integral gain
$k_{i,q}$	quadrature component of the integral gain
$k_{p,d}$	direct component of the proportional gain
$k_{p,q}$	quadrature component of the proportional gain
L_d	direct synchronous inductance
L_q	quadrature synchronous inductance
L_s	stator synchronous inductance
n	speed in rpm
P_1	input power of the motor
P_2	output power of the motor
p	number of pair poles
P_{acd1}	input power of the motor controller
P_d	power dissipation

P_{Loss}	sum of on-state losses and the average switching losses
P_{loss}	motor power losses
Q	rate of transfer heat between two parts
q_c	heat transfer by conduction
q_h	heat transferring by convection
q_r	heat transfer by radiation
R	thermal resistance
R_s	stator resistance per phase
$R_{\theta cs}$	thermal resistance case-sink
$R_{\theta ja}$	thermal resistance junction-ambient
$R_{\theta jc}$	thermal resistance junction-case
$R_{\theta sa}$	thermal resistance sink-ambient
T_a	ambient temperature
$T_{a,max}$	maximum ambient temperature
T_e	electromagnetic torque
T_j	junction temperature
$T_{j,max}$	maximum junction temperature
T_m	mechanical torque
t_r	rise time of the current step response
T_s	surface temperature
u_{dc}	dc-link voltage
u_{max}	maximum stator voltage
V_{an}	voltage in phase a
V_{bn}	voltage in phase b
V_{cn}	voltage in phase c
V_d	direct stator voltage
V_{pp}	phase to phase voltage
V_q	quadrature stator voltage
ΔT	temperature gradient
α_c	closed loop bandwidth
α_s	angle of the stator current vector
β	torque angle
η_acd	motor controller efficiency
η_m	motor efficiency
ω	angular speed
ω_e	electric speed in rpm
ψ_d	direct flux component
ψ_m	permanent magnet flux linkage
ψ_q	quadrature flux component
ρ	electrical resistivity, density

σ	Stephan-Boltzmann constant
θ	transformation angle
θ_r	rotor angle

Subscripts

a	phase a component
b	phase b component
c	phase c component
d	direct-axis component
max	maximum
mean	mean value
min	minimum
q	quadrature-axis component
r	rated value
ref	reference value
surf	surface

Abbreviations

dc	direct current
fund.	fundamental
max	maximum
min	minimum
ref	reference
rms	root mean square
sinu.	sinusoidal
spec.	specification
ACD	AC Drive/Motor Controller
ACM	Autonomous Corner Modules
BEV	Battery Electric Vehicle
BEMF	Back Electromotive Force
BMU	Battery Management Unit
CAN	Control Area Network
CANH	High Level Transmission Line
CANL	Low Level Transmission Line
CAL	CAN Application Layer
COB-ID	CAN object Identifier
DBT	Distributor
DTC	Direct Torque Control
ECU	Electronic Control Units
EPS	Electric Power Steering

EV	Electrical Vehicle
FOC	Field-Oriented Control
ICEV	Internal combustion engine vehicle
ID	Identifier
LIN	Local Interconnect Network)
LLC	Logical Link Control
LMT	Layer Management
MAC	Multiple Access Control
MOST	Media Oriented Systems Transport
NMT	Network Management
OD	Object dictionary
PCM	Powertrain Control Module
PDO	Process Data Object
PMSM	Permanent Magnet Synchronous Machine
PWM	PulseWidthModulation
RCV	Research Concept Vehicle
SDO	Service Data Object
SYNC	Synchronization
TM	Transmission

References

[1] "Advanced motion controls, rev 3.0.3a ,300 series canopen drives."

[2] M. Asadi and B. Arezi, "Thermal design, modeling and simulation of air forced cooling heat sink for thyristor controlled reactor (tcr)," *IEEE Power Electronics*, pp. 625–631, 2011.

[3] H. Boterenbrood, "Canopen high-level protocol for can-bus," March, Amsterdan 2000.

[4] S. Chi, "Position-sensorless control of permanent magnet synchronous machines over wide speed range," Doctoral Thesis, The Ohio State University, 2007.

[5] Y. Chin and J. Soulard, "A permanent magnet synchronous motor for traction applications of electric vehicles," *IEEE International Electric Machines Drives Conference (IEMDC),*, 2003.

[6] (2008) dspace microautobox. [Online]. Available: http://www.dspace.de/shared/data/pdf/flyer2008/dspace_2008_microautobox_en_pi480.pdf

[7] M. Felden, P. Butterling, P. Jeckand, L. Eckstein, and K. Hameyer, "Electric vehicle drive trains: From the specification sheet to the drive-train concept," *14th International Power Electronics and Motion Control Conference, EPE-PEMC*, pp. S11–9 to S11–16, 2010.

[8] S. Haghbin, "Integrated motor drives and battery chargers for electric or plug-in hybrid electric vehicles," Doctoral Thesis, Chalmers University of Thechnology, Sweden, Gothenburg, 2013.

[9] Ifedi, Mecrow, Brockway, Boast, Atkinson, and Kostic-Perovic, "Fault tolerant in-wheel motor topologies for high performance electric vehicles." *IEEE International Electric Machines Drives Conference (IEMDC)*, pp. 1310–1315, 2011.

[10] A. K. Jain and V. T. Ranganathan, "Modeling and field oriented control of salient pole wound field synchronous machine in stator flux coordinates," *IEEE Transactions on Industrial Electronics*, pp. 960–970, March 2011.

[11] M. P. Kazmierkowski and L. Malesani, "Current control techniques for three-phase voltage-source pwm converters: A survey," *IEEE Transactions on Industrial Electronics*, pp. 691–703, October 1989.

[12] R. K.M., P. N.R., W. T.G., N. M.J., C. F., and Crescimbini, "Application of direct-drive wheel motor for fuel cell electric and hybrid electric vehicle propulsion system," *IEEE Transaction on Industry Applications*, pp. 1186–1189, September 2006.

[13] S. Lee, "Optimum design and selection of heat sinks," *IEEE Transactions on Industrial Electronics*, pp. 48–54, 1995.

[14] N. Mohan, T. M. Undeland, and W. P. Robbins, Eds., *Power Electronics: Converters, Applications, and Design*. Jonh Wiley e Sons, INC.

[15] Olaf, P. Andrew, A. Christian, and K., "Embedded networking with can and canopen," 2004.

[16] S. R. Perez, "Analysis of a light permanent magnet in-wheel motor for an electric vehicle with autonomous corner modules," Master Thesis, Royal Institute of Technology: KTH University, Sweden, Stockholm, February 2011.

[17] L. Ran, W. Junfeng, W. Haiying, and L. Gechen, "Design method of can bus network communication structure for electric vehicle," *Strategic Technology (IFOST), 2010 International Forum*, pp. 1–4, 2010.

[18] (2012) Kth research concept vehicle. [Online]. Available: http://www.kth.se/en/forskning/forskningsplattformar/transport/initiativ/t-labs/projects

[19] C. Sadarangani, Ed., *Design and Analysis of Induction and Permanent Magnet Motors*. Stockholm: KTH, 2006.

[20] P. Vas, Ed., *Sensorless Vector And Direct Torque Control*. University of Aberdeen: Oxford Science Publications, 1989.

[21] O. Wallmark, "On control of permanent-magnet synchronous motors in hybrid-electric vehicle applications," Licentiate Thesis, Chalmers University of Technology, Sweden, Goteborg, 2004.

[22] X. Wang, N. Liu, , and R. Na, "Simulation of pmsm field-oriented control based on svpwm," *IEEE Vehicle Power and Propulsion Conference*, pp. 1465–1469, 2009.

[23] Y. Yang, J. Liang, and X. Xing, "Design and application of axial-flux permanent magnet wheel motors for an electric vehicle," *IEEE AFRICON,*, pp. 1–5, September 2009.

[24] S. Z., “Electromechanical steering, suspension drive and brake modules,” *56th IEEE Vehicular Technology Conference*, pp. 1856–1863, September 2002.

[25] M. Zeraoulia, M. Benbouzid, and D. Diallo, “Electric motor drive selection issues for hev propulsion systems: A comparative study,” *IEEE Conference on Vehicle Power and Propulsion*, pp. 1756–1764, 2005.

[26] S. Zetterstrom, “Vehicle wheel suspension arrangement,” Patent EP1 144 212, 1998.